

Quantifying the Impacts of Marine Aerosols over the Southeast Atlantic Ocean using a chemical transport model: Implications for aerosol-cloud interactions

Mashiat Hossain¹, Rebecca M. Garland², Hannah M. Horowitz¹

¹Civil and Environmental Engineering, University of Illinois Urbana-Champaign, IL, USA

²Department of Geography, Geoinformatics and Meteorology, University of Pretoria, Pretoria, South Africa

Correspondence to: Mashiat Hossain (mashiat3@illinois.edu), Hannah M. Horowitz (hmhorow@illinois.edu)

Abstract. The southeast Atlantic region, characterized by persistent stratocumulus clouds, has one of the highest uncertainties in aerosol radiative forcing and significant variability across climate models. In this study, we analyze the seasonally varying role of marine aerosol sources and identify key uncertainties in aerosol composition at cloud-relevant altitudes over the southeast Atlantic using the GEOS-Chem chemical transport model. We evaluate simulated aerosol optical depth (AOD) and speciated aerosol concentrations against those collected from ground observations and aircraft campaigns such as LASIC, ORACLES, and CLARIFY, conducted during 2017. The model consistently underestimates AOD relative to AERONET, particularly at remote locations like Ascension Island. However, when compared with aerosol mass concentrations from aircraft campaigns during the biomass burning period, it performs adequately at cloud-relevant altitudes, with a normalized mean bias (NMB) between -3.5% (CLARIFY) and -7.5% (ORACLES). At these altitudes, in the model organic aerosols (63%) dominate during the biomass burning period, while sulfate (41%) prevails during austral summer, when dimethylsulfide (DMS) emissions peak in the model. Our findings indicate that marine sulfate can account for up to 69% of total sulfate during high DMS period. Sensitivity analyses indicate that refining DMS emissions and oxidation chemistry may increase sulfate aerosol produced from marine sources, highlighting that there remains large uncertainty in the role of DMS emissions in the marine boundary layer. Additionally, we find marine primary organic aerosol emissions may substantially increase total organic aerosol concentrations, particularly during austral summer. This study underscores the imperative need to refine marine emissions and their chemical transformations, as aerosols from marine sources are a major component of total aerosols at cloud-relevant altitudes and may impact uncertainties in aerosol radiative forcing over the southeast Atlantic.

1 Introduction

Marine aerosols are a primary contributor to natural atmospheric aerosols, and consequently influence the Earth's radiative balance (Spracklen et al., 2008; Vignati et al., 2001). Aerosols in the marine boundary layer have significant impact on the properties of low-altitude marine clouds, particularly their ability to reflect solar radiation and cool the climate (Seinfeld and Pandis, 2016; Wood, 2012; Chen et al., 2014; Quinn et al., 2017). The southeast Atlantic (SEA) is marked by a persistent deck of low-level stratocumulus (Sc) clouds. However, this region exhibits highest uncertainty in aerosol radiative forcings in the AeroCom intercomparison across CMIP5 general circulation models (GCMs) and chemical transport models (Stier et al., 2013). This uncertainty is primarily driven by challenges in

34 accurately representing cloud fraction, aerosol-cloud properties, and vertical structure, both in the presence and
35 absence of smoke (Stier et al., 2013; Doherty et al., 2022). In this study, we investigate the role of marine aerosols
36 and sources of uncertainty affecting aerosol composition within the boundary layer, particularly in this critical region
37 of aerosol-cloud interactions over the SEA.

38 The SEA region encompasses the Benguela upwelling system (BUS), renowned for its high primary production of
39 marine phytoplankton and fish populations (Shannon and Nelson, 1996; Jarre et al., 2015). This elevated
40 phytoplankton activity serves as the main natural source of the volatile organic compound dimethylsulfide (DMS),
41 thereby influencing the global tropospheric sulfur budget (Andreae, 1990; Bates et al., 1992). Once released into the
42 atmosphere through air-sea exchange, DMS undergoes complex chemical transformations. In the gas phase, it is
43 oxidized to form H_2SO_4 and methanesulfonic acid (MSA), which has implications for new particle formation (Chen
44 et al., 2015); while in the aqueous phase, it leads to the production of MSA and sulfate aerosols, impacting cloud
45 microphysical properties (Kaufman and Tanré, 1994). Although DMS is a critical source of natural aerosols,
46 contributing over 50% of natural gas-phase sulfur emissions (Chin et al., 1996; Kilgour et al., 2021), the exact
47 mechanisms of DMS oxidation and subsequent formation of sulfate and MSA aerosol remain inadequately understood
48 (Ravishankara et al., 1997; Barnes et al., 2006; Hoffmann et al., 2016). This gap in understanding contributes to
49 substantial uncertainty in aerosol radiative forcing, which is highly sensitive to uncertainties in natural aerosols
50 (Carslaw et al., 2013; Fung et al., 2022). Additionally, marine aerosols comprise primary aerosols such as sea spray
51 aerosols, which consist of salts, sulfate, and organic matter, released into the atmosphere primarily by the bubble-
52 bursting process (O'Dowd and De Leeuw, 2007; Russell et al., 2010; Prather et al., 2013; Brooks and Thornton, 2018;
53 Russell et al., 2023). Investigating the uncertainties related to marine emissions and chemistry are crucial to refine our
54 understanding of the impacts of marine aerosols on climate.

55 The SEA lies at the confluence of not only marine aerosols, but other natural and anthropogenic aerosols from local
56 and distant origin (Andreae et al., 1995; Swap et al., 1996; Formenti et al., 1999; Swap et al., 2003; Tournadre, 2014).
57 During the austral spring (August to October), seasonal fires in the neighboring southern African region contribute
58 nearly one-third of global total biomass burning emissions (van der Werf et al., 2010). This seasonal influx of biomass
59 burning aerosols aloft interacts with the underlying Sc deck, introducing considerable variability into aerosol forcing
60 assessments in the SEA region (Lindesay et al., 1996; Swap et al., 2003). To address these uncertainties, several
61 international field campaigns were conducted between 1992 and 2018 during the peak biomass burning season (Swap
62 et al., 2003; Formenti et al., 2019; Haywood et al., 2021; Redemann et al., 2021). Despite the region being a prolific
63 source of marine aerosols throughout the year, the potential impact of aerosols on regional climate dynamics through
64 interactions with the persistent low-level marine clouds outside of the biomass burning season has been largely
65 overlooked.

66 Here, we use the GEOS-Chem global chemical transport model to analyze high-resolution, seasonally varying aerosol
67 composition at the altitudes of persistent stratocumulus clouds over the SEA. We specifically focus on the role of
68 marine aerosols, analyzing their contributions to sulfate and organic aerosol concentrations. We evaluate simulated

69 aerosol optical depth (AOD) and speciated aerosol concentrations against observational data from the Aerosol Robotic
70 Network (AERONET) and the Layered Atlantic Smoke Interactions with Clouds (LASIC; Zuidema et al., 2018),
71 Observations of Aerosols above Clouds and their interactionS (ORACLES; Redemann et al., 2021), and Cloud-
72 Aerosol-Radiation Interaction and Forcing (CLARIFY; Haywood et al., 2021) field campaigns during the year 2017.
73 We assess the sensitivity of our results to uncertainty in DMS oxidation mechanisms and emissions of DMS, SO₂, and
74 marine primary organics. Our findings aim to enhance understanding of the seasonally varying role of marine aerosols
75 in aerosol-cloud interactions in the SEA by a comprehensive evaluation of aerosol composition at cloud altitudes.

76 **2 Methodology**

77 **2.1 Model Description**

78 Here, we use the GEOS-Chem 3D atmospheric chemical transport model version 13.3.3 with detailed gas- and aerosol-
79 phase tropospheric chemistry (<https://zenodo.org/records/5748260>). The model is driven by meteorology from the
80 Modern-Era Retrospective Analysis for Research and Applications, Version-2 (MERRA2) reanalysis, from the NASA
81 Global Modeling Assimilation Office (GMAO) (Gelaro et al., 2017). We perform nested grid simulations over the
82 southwestern coast of Africa (40°W-20°E, 0-40°S) with a horizontal resolution of 0.5° by 0.625° and extending over
83 47 vertical layers from the surface to 0.01hPa. A chemical time step of 20 minutes and transport time step of 10
84 minutes is applied, as recommended by Philip et al. (2016). Prior to the target year, 2017, we conduct a 6-month spin-
85 up simulation. Boundary conditions are obtained from global simulations performed at 4° latitude × 5° longitude
86 horizontal resolution for the same year after a 6-month initialization.

87 In GEOS-Chem, carbonaceous aerosol includes organic aerosols (OA) and black carbon (BC). Organic aerosol is
88 simulated using the “simple” scheme which treats primary organic aerosol (POA) as non-volatile and includes
89 irreversible direct yield of SOA from precursors (Pai et al., 2020). The BC simulation follows the methodologies of
90 Park et al. (2003) and Wang et al. (2014). Sulfate (Alexander et al., 2009), nitrate (Jaeglé et al., 2018), and ammonium
91 (Fountoukis and Nenes, 2007) thermodynamic partitioning is estimated using the ISORROPIA II thermodynamic
92 model (Fountoukis and Nenes, 2007). Monthly anthropogenic emissions follow the Community Emissions Data
93 System (CEDSv2) inventory (Hoesly et al., 2018). Biomass burning emissions are calculated using the Global Fire
94 Emissions Database (GFED4.1s) at 0.25°×0.25° spatial resolution, with fractional daily and 3-hourly scaling factors
95 applied to the cumulative monthly data (van der Werf et al., 2017). DMS emissions in the standard model use the Lana
96 et al. (2011) climatology, which compiles DMS concentrations using data from the Global Surface Seawater DMS
97 Database (<http://saga.pmel.noaa.gov/dms/>) collected from 1972 to 2009, incorporated with additional observations
98 from the South Pacific (Lee et al., 2010). The standard DMS oxidation mechanism in the model includes only three
99 gas-phase DMS reactions, which directly yield SO₂ and MSA according to the reaction mechanism outlined by Chin
100 et al. (1996), and incorporates updated reaction rate coefficients from Burkholder et al. (2015). Sea-salt aerosol (SSA)
101 emissions from the open ocean are both windspeed- (Gong et al., 2003) and sea surface temperature-dependent (Jaeglé
102 et al., 2011). Dust emissions include natural dust (Fairlie et al., 2007) and anthropogenic dust from the AFCID
103 inventory (Philip et al., 2017).

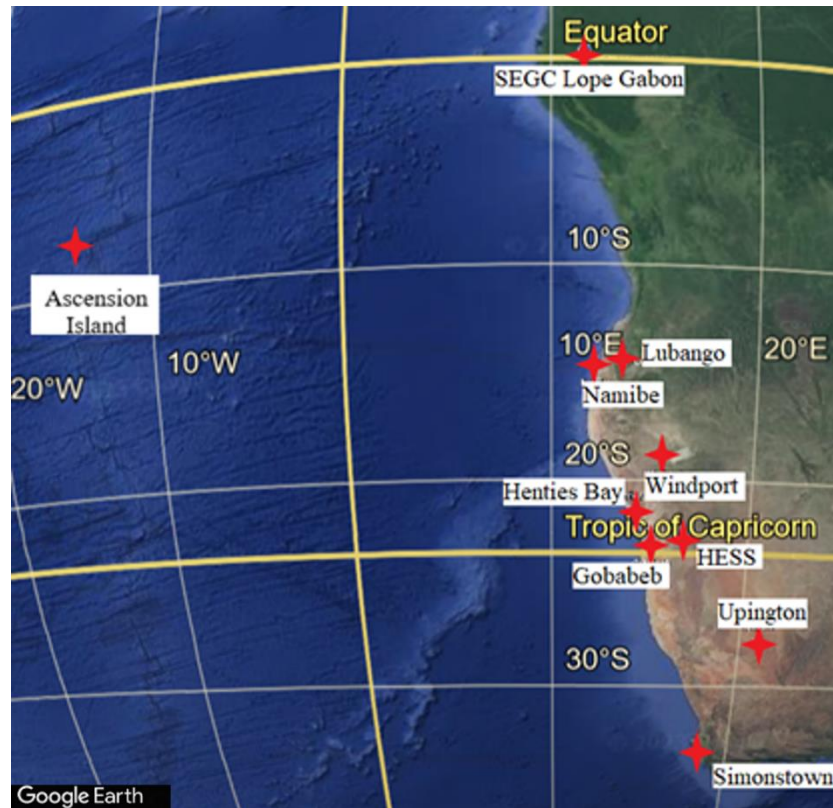
104 In this study, we carry out multiple simulations to explore the sensitivity of marine aerosols to various emission
105 sources. To quantify the impact of marine sources on sulfate aerosols within the stratocumulus cloud layer, we perform
106 a high-resolution ($0.5^\circ \times 0.625^\circ$) marine emissions only sensitivity simulation where SO_2 and SO_4 emissions from
107 anthropogenic sources, biomass burning, volcanic activity, ships and aviation were turned off. Additionally, to
108 investigate the sensitivity of DMS emission fluxes to surface ocean DMS concentrations, we perform an additional
109 simulation with DMS concentrations from Galí et al. (2018). In this dataset, DMS concentrations are estimated through
110 a remote-sensing algorithm that integrates satellite-derived estimates of chlorophyll and light penetration, along with
111 climatological mixed layer depth (Galí et al., 2018). Furthermore, we assess the impact of adding marine POA, co-
112 emitted with sea-salt aerosols (Gantt et al., 2015), on the overall organic aerosol burden, which is not included in the
113 standard model configuration. Finally, to evaluate how uncertainty in biomass burning SO_2 emissions affects the
114 relative importance of marine emissions to sulfate aerosol, we conduct two sets of sensitivity simulations using the
115 Quick Fire Emissions Dataset (QFED) (Darmenov & da Silva, 2013; Das et al., 2017), and the Global Fire
116 Assimilation System (GFAS) (Kaiser et al., 2012; Su et al., 2023). Each of these inventories differ in data sources,
117 methodology, temporal resolution and plume injection height. These sensitivity analyses were conducted for the year
118 2017, following a six-month spin-up period. Details regarding the spatial resolution used in each sensitivity analysis
119 are provided in Table A1.

120 2.2 Ground-based measurements

121 We evaluate simulated aerosol optical depth (AOD) against AOD retrieved from the ground-based Aerosol Robotic
122 Network (AERONET) of sun photometers with direct sun measurements every 15 min (Holben et al., 1998). We use
123 Level 2.0 Version 3 data that have improved cloud screening algorithms (Giles et al., 2019). We strategically select
124 nine sites in the study domain along coastal and oceanic regions, as shown in Fig. 1. Site information, including the
125 coordinates, number of months with available data and the monthly average AOD for three distinct time periods, is
126 summarized in Table A2. The AERONET monthly average AOD is computed from daily averages for sites with at
127 least 3 months of observations during the model simulation period (year 2017) and months with at least 15 days of
128 measurements. These are then compared with the monthly mean AOD from the GEOS-Chem model.

129 The modeled AOD is sampled at each AERONET site location and computed at 550 nm wavelength by vertically
130 integrating scattering and absorption coefficients based on the properties of various aerosol components, such as size
131 distributions, hygroscopicity, refractive indices, and densities (Latimer and Martin, 2019). For comparison with
132 modeled monthly AOD, daily measurements at each site at 440 nm are first interpolated to the standard wavelength
133 of 550 nm using the local Ångström exponent between 440 and 870 nm channels, following the Ångström power law
134 (Eq. (1); Martínez-Lozano et al., 1998). These interpolated values are then averaged to calculate the observed mean
135 monthly AOD. The interpolation formula used is:

$$136 \quad AOD_{(550nm)} = AOD_{(440nm)} * \left(\frac{550}{440}\right)^{-\alpha_{\text{ext}}\left(\frac{440}{870}\right)} \quad (1)$$



137

138 **Figure 1: Map of AERONET sites used for model evaluation (© Google Earth).**

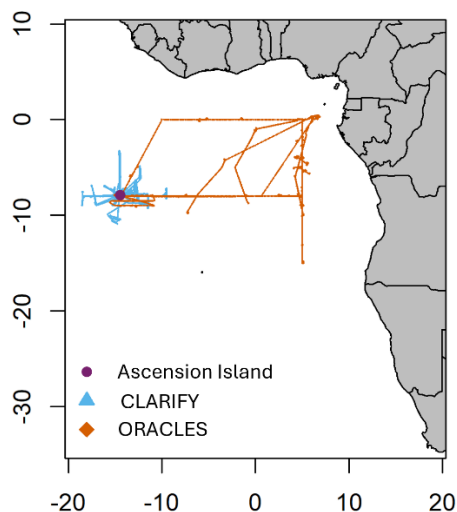
139 In addition, we evaluate the model's relative aerosol composition against measurements from the Atmospheric
 140 Radiation Measurement (ARM) facility on Ascension Island during the LASIC campaign, conducted from January to
 141 November 2017. LASIC employed an Aerodyne aerosol chemical speciation monitor (ACSM) to provide quantitative
 142 measurement of the chemical composition of non-refractory aerosol components including sulfate, nitrate,
 143 ammonium, and organics. For comparative analysis, we use aerosol concentrations corrected for composition-
 144 dependent collection efficiency (CDCE) obtained from the ARM Data Archive. Barrett et al. (2022) reported that
 145 aerosol mass concentrations of individual components observed by the LASIC ACSM were 2 to 4.5 times lower than
 146 those measured by the aerosol mass spectrometer (AMS) aboard the CLARIFY campaign aircraft. Hence, we evaluate
 147 the relative rather than absolute aerosol speciation in GEOS-Chem against the LASIC ACSM.

148 **2.3 Aircraft measurements**

149 We evaluate simulated aerosol composition against airborne measurements from two campaigns, NASA ORACLES
 150 (Redemann et al., 2021; Ryoo et al., 2021) and UK CLARIFY (Haywood et al., 2021). The ORACLES field campaign
 151 used the NASA P-3 aircraft to make measurements based out of São Tomé and Príncipe while CLARIFY used the
 152 FAAM BAe-146 aircraft around Ascension Island for data collection. The ORACLES aircraft primarily conducted
 153 morning sampling, between 8:00-13:00 UTC, while the CLARIFY aircraft often sampled extended hours, typically
 154 from 7:00-18:00 UTC. Both campaigns occurred during the austral winter/spring (August-September), corresponding

155 with peak biomass burning events in southern Africa (Adebiyi et al., 2015). Figure 2 shows the flight tracks for these
 156 campaigns. The primary instruments and references for each campaign are listed in Table 1.

157



158

159 **Figure 2: Flight tracks from the two aircraft campaigns used to evaluate the model, CLARIFY (in blue) and ORACLES**
 160 **(in orange), conducted during August-September 2017 over the southeast Atlantic region. Ascension Island is marked by**
 161 **the purple dot.**

162 To facilitate comparison between airborne measurements and the GEOS-Chem model, we sampled the model to the
 163 nearest grid box, both temporally and spatially, along the flight tracks. Observations from both campaigns are reported
 164 at 1-minute averaging intervals, while the model operates at a 10-minute temporal resolution (see Sect. 2.1). Aerosol
 165 concentrations from the campaigns are reported as mass concentrations at standard temperature and pressure (STP:
 166 273 K, 1 atm). The modeled concentrations are thus also standardized to STP conditions.

167 **Table 1: Aircraft campaigns in the southeast Atlantic used for model evaluation during the biomass burning season**

Campaign	Date range (Duration)	Instruments*	Aerodynamic Diameter (μm)	Altitude from surface (km)	Primary Reference
CLARIFY	7 th August–4 th September 2017 (99h)	C-ToF-AMS	0.05 to 0.60	0 to 8	Haywood et al., 2021

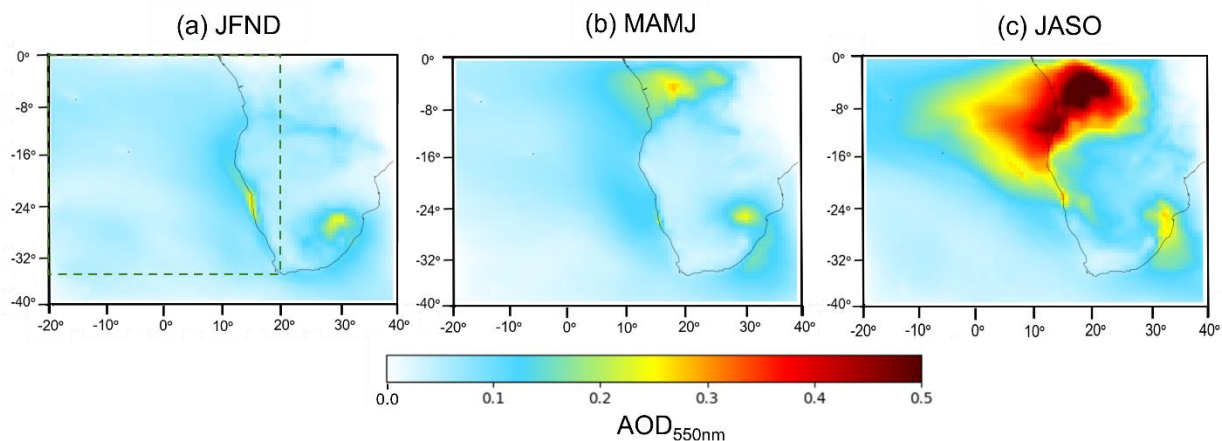
ORACLES	16 th August–6 th September 2017 (112h)	HR-ToF- AMS	0.07 and 0.70	0 to 7	Redemann et al., 2021
---------	---------------------------------------------------------------------	----------------	---------------	--------	--------------------------

168 *Compact Time-of-Flight (C-ToF), High Resolution Time-of-Flight (HR-ToF), Aerosol Mass Spectrometer (AMS)

169 3.1 Model Evaluation

170 3.1.1 Seasonal variation of AOD

171 The spatial distribution of seasonal mean AOD from GEOS-Chem for the year 2017 is presented in Fig. 3. Three
 172 distinct seasonal periods reflect dominant atmospheric and oceanic processes. These include the high DMS emission
 173 period in the SEA, during the months of January, February, November, and December (JFND); the peak biomass
 174 burning season in southern Africa, spanning from July to October (JASO); and the transitional season, encompassing
 175 March, April, May, and June (MAMJ).

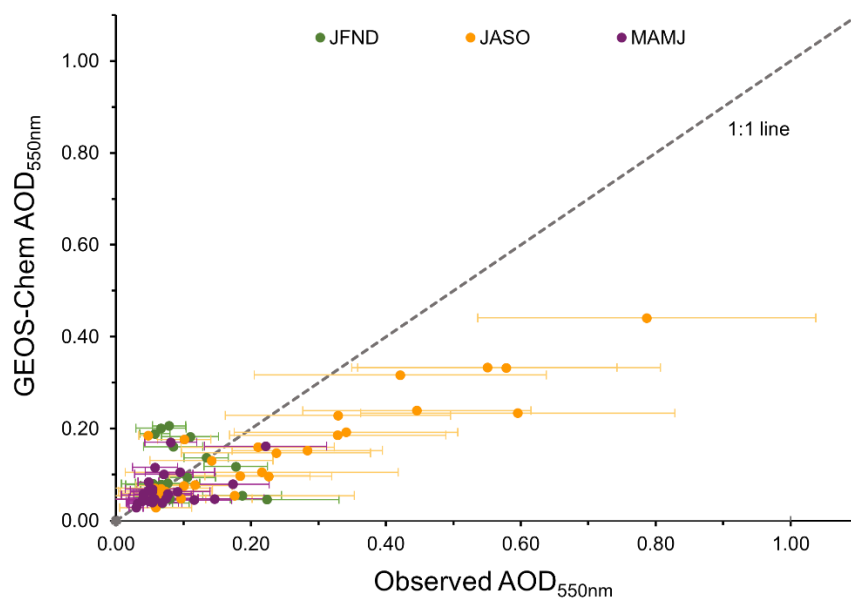


176
 177 **Figure 3: Spatial distribution of seasonal mean modeled AOD at 550 nm for 2017. Seasons are as follows: (a) the peak DMS**
 178 **emission period (JFND), (b) the transitional period (MAMJ), and (c) the peak biomass burning period (JASO). The sub-**
 179 **domain (0–35° S, 20° E–20° W) is highlighted with a green dotted rectangle in panel (a) for reference.**

180 The simulated DMS emissions, based on Lana climatology (2011), indicates that emissions in the BUS region peak
 181 in January, leading to elevated concentrations of sulfate aerosols. This increased sulfate (~20%), combined with dust
 182 (59%) emissions from the Namib desert, contributes to an AOD hotspot as depicted in Fig. 3a on the southwestern
 183 coast. In the JASO period (Fig. 3c), modeled AOD increases due to biomass burning aerosols, originating from
 184 savannah fires in Central and southern Africa and transported westward towards the SEA region by the southern
 185 African easterly jet (Adebiyi and Zuidema, 2016). The spatial distribution of mean transitional period AOD (Fig. 3b)
 186 features hotspots in Congo and Angola which coincide with the onset of biomass burning in Central Africa.
 187 Additionally, a year-round AOD hotspot is observed in northeastern South Africa (Gauteng province; Fig. 3), which
 188 is associated with elevated aerosol concentrations due to industrial and mining activities, as well as domestic fuel
 189 burning (Arowosegbe et al. 2021; Zhang et al. 2021).

190

191



192

193 **Figure 4: Modeled AOD_{550nm} (Y-axis) with respect to AERONET AOD_{550nm} (X-axis). Each data point represents the**
194 **monthly mean values for each station color-coded by season (green- DMS period, yellow - biomass burning period, purple-**
195 **transitional period). Error bars indicate the standard deviation of the AERONET AOD_{550nm} values, and the dotted line**
196 **depicts the 1:1 relationship.**

197 Figure 4 shows the correlation of monthly average AERONET and GEOS-Chem AOD across the nine selected sites
198 (see Sect. 2.1 and Fig. 1), with the three seasonal periods distinguished by color: green for peak DMS emission season
199 (JFND), yellow for biomass burning season (JASO), and purple for the transition period (MAMJ). Each data point
200 corresponds to the monthly mean AOD values at distinct AERONET sites. The error bars in Fig. 4 represent the ± 1
201 standard deviation in monthly AOD measurements at these sites, with higher deviations observed during the biomass
202 burning months (up to ± 0.25 at Namibe site). The comparison of monthly mean AOD across individual sites (see
203 Table A2 in the Appendix) shows that, with the exception of Ascension Island, Gobabeb, and Upington, the mean
204 AOD at the remaining sites during the biomass burning season (JASO) is at least one standard deviation higher than
205 the mean AOD in other seasons (JFND & MAMJ).

206 Table 2 compiles the performance of monthly mean GEOS-Chem AOD with respect to AERONET AOD by season.
207 JASO exhibits the strongest correlation ($R = 0.901$), which is statistically significant ($p < 0.05$). The transitional period
208 (MAMJ) shows a moderate correlation ($R = 0.48$) with a normalized mean bias (NMB) of 4.5%. Negligible negative
209 correlation coefficient ($R = -0.058$) with a positive bias (29.8%) is seen during the summer period (JFND),
210 predominantly due to anomalies at two sites. This period witnesses a considerable underestimation of AOD at
211 Ascension Island, alongside an overestimation of dust aerosol at Gobabeb. Excluding these two sites, improves the

212 model's correlation to 0.67 ($p = 0.55$) and reduces the NMB to 4.7%. This underestimate of AOD at Ascension Island
 213 (Fig. A1 in the Appendix) during summer (JFND) suggests potential model limitations in accurately simulating natural
 214 aerosol emissions such as sea salt and marine biogenic emissions. Meanwhile, the AOD discrepancy at Ascension
 215 Island in the biomass burning season, may be due to the underestimate of transatlantic transport of light-absorbing
 216 carbon aerosols (Das et al., 2017) and deviations in its spatial distribution from typical zonal patterns over the Atlantic
 217 (Adebiyi et al., 2023). The sources of these model biases are discussed in further detail in Section 3.1.2.

218 Table 2: Statistical parameters of monthly mean modeled AOD with respect to observed AOD at the AERONET sites
 219 by season

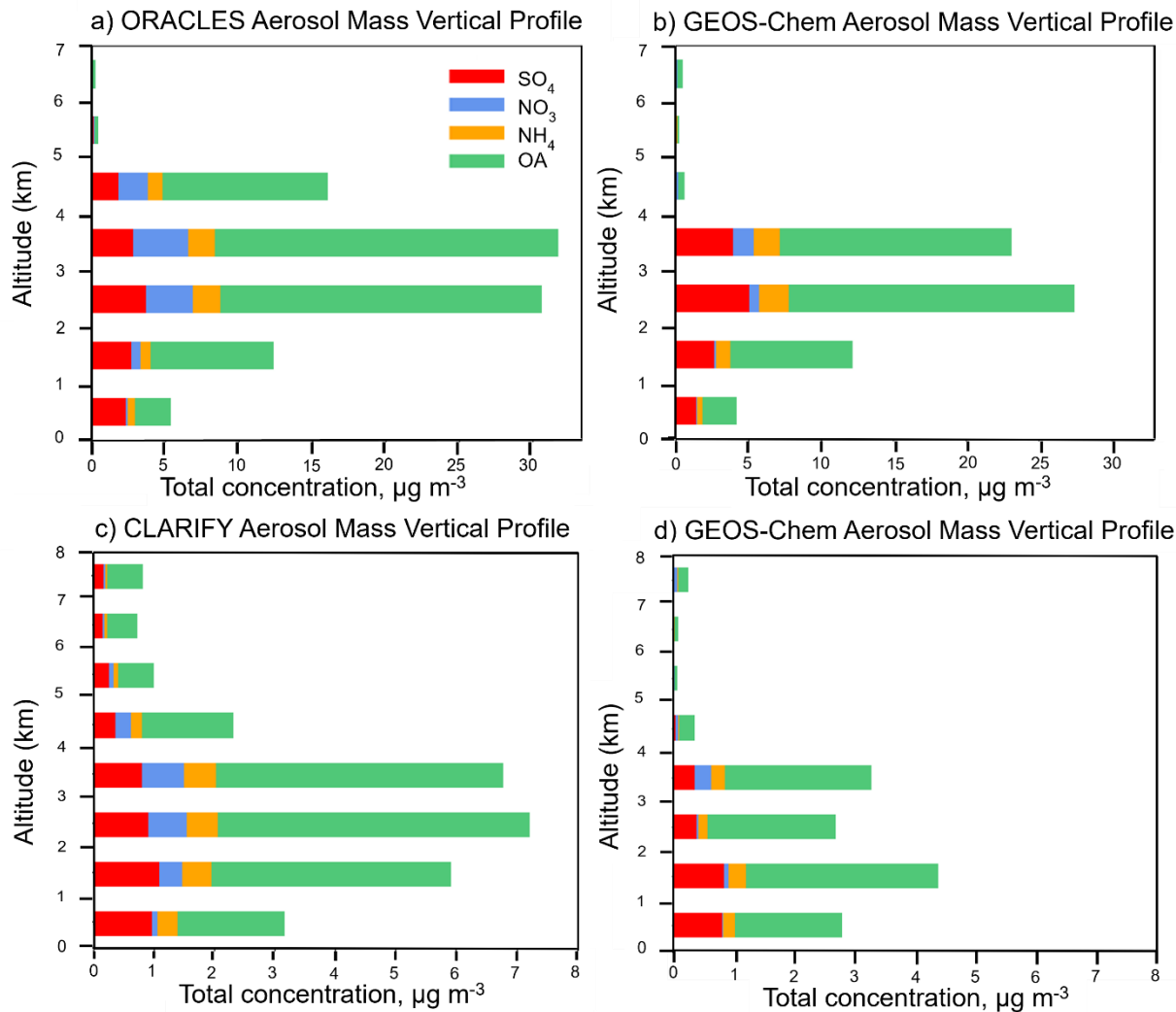
Time period	Number of observations	Correlation coefficient (R)	Normalized mean bias (NMB) (%)	Root-mean square error (RMSE)
JFND	20	-0.058 ($p = 0.62$)	29.8	0.079
MAMJ	26	0.48 ($p = 0.59$)	4.5	0.043
JASO	28	0.901 ($p = 0.044$)	-18.6	0.15

220 We evaluate the relative aerosol speciation simulated at Ascension Island against monthly mean ACSM observations
 221 during the LASIC campaign (see Sect. 2.2) available for January–November 2017 (Fig. A2 in the Appendix). The
 222 seasonality of the relative contributions of organic aerosols and sulfate are consistent between the model and
 223 observations. However, the model underestimates the relative contribution of sulfate during most months, while
 224 generally overestimating the proportion of organics. An increase in the transport of biomass burning organic aerosols
 225 would further worsen the model underestimate of sulfate. A slight overestimate in the modeled relative contribution
 226 of sulfate is observed in February, and November, when simulated DMS emissions in the region are high (Lana et al.,
 227 2011), largely due to enhanced underestimations of organics and nitrates.

228 3.1.2 Vertical profiles of aerosol composition

229 Figure 5 depicts the mean vertical profiles of speciated aerosol mass concentrations observed during ORACLES and
 230 CLARIFY aircraft campaigns in August–September 2017 (the biomass burning season), compared to GEOS-Chem
 231 (see Sect. 2.2 and Table 1). The cloud top height in the SEA region generally falls between 0 to 2 km (Redemann et
 232 al., 2021). Findings from Diamond et al. (2018) indicate that aerosols below clouds in this lower atmospheric layer
 233 can also substantially impact cloud microphysics. At these altitudes (0–2 km), GEOS-Chem performs well against
 234 AMS measurements of total aerosol mass, which includes sulfate, nitrate, ammonium and organics from these
 235 campaigns, with an NMB between -3.5% (CLARIFY) to -7.5% (ORACLES). At mid-altitudes (2–4 km), the model

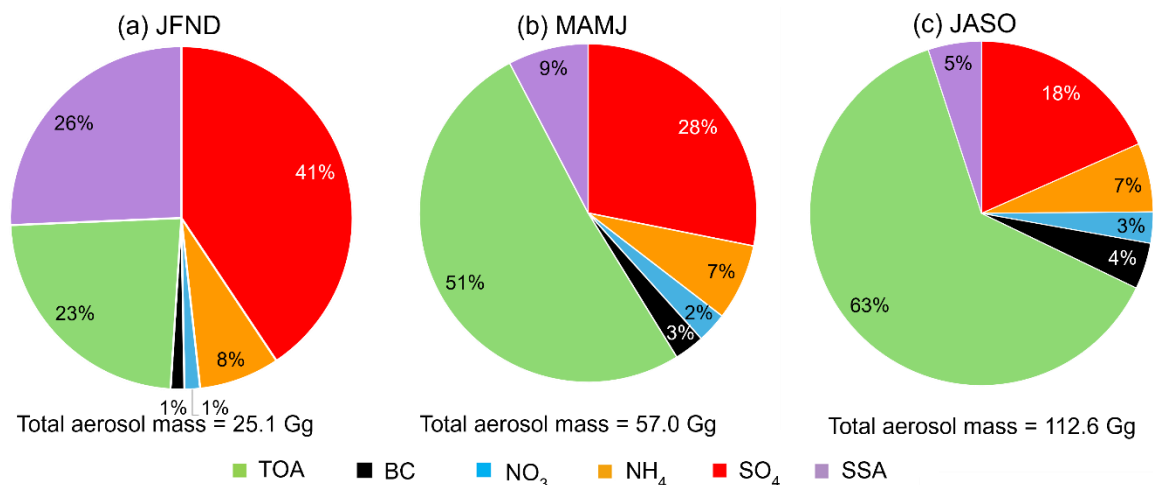
236 is biased low, with NMB values spanning -19% (ORACLES) to -57% (CLARIFY). However, the model demonstrates
237 a pronounced bias at higher altitudes (4–7 km), where NMB values drop to -92% (ORACLES) to -93.5% (CLARIFY),
238 underscoring challenges in accurately modeling aerosol concentrations at these elevations. These significant low
239 biases in aerosol concentrations at higher altitude likely contribute to the model’s underestimation of AOD during the
240 biomass burning period (see Section 3.1.1). This underestimation may also be affected by the model’s bulk aerosol
241 scheme, which inadequately captures the optical properties of aerosols and is compounded by a low relative humidity
242 bias (Zhai et al., 2021). The bulk scheme also assumes all aerosols are externally mixed, which contrasts with the
243 variable degree of particle mixing states in the atmosphere (Yu et al., 2012; Dang et al., 2022). Moreover, studies like
244 Hodzic et al. (2020) using NASA ATom aircraft data indicate that GEOS-Chem substantially underestimates oxidation
245 levels of organic aerosols in remote areas, which could affect estimates of their burden and optical properties. Pai et
246 al. (2020) further suggests that the model underestimation of organic aerosol loading at mid-tropospheric heights is
247 linked to the surface injection treatment of fire emissions in GFED4.1s. Recent studies by Wizenberg et al. (2023) and
248 Marvin et al. (2024) concur that fire injection scheme is a critical source of model uncertainty, emphasizing the
249 potential importance of accurate fire injection modeling in the free troposphere. Nonetheless, our study focuses on
250 aerosol composition within cloud-relevant altitudes to improve our understanding of aerosol-cloud interactions and
251 their climate implications. The observed vertical distribution of aerosol mass concentrations (left panels of Fig. 5),
252 indicates that 18% and 36% of the aerosol mass for the ORACLES and CLARIFY campaigns, respectively, is located
253 below 2 km, within columns extending up to flight altitudes of 7 km and 8 km. However, the model simulates elevated
254 aerosol mass at these lower altitudes, 24% and 50% of the column for ORACLES and CLARIFY, respectively.



255
 256 **Figure 5: Average vertical profiles of simulated and observed aerosol mass during August–September 2017 (peak biomass**
 257 **burning season) from aircraft campaigns. The left column presents the vertical distribution of aerosols observed during the**
 258 **ORACLES flight campaign (panel a) and the CLARIFY flight campaign (panel c) at STP (see Sect. 2.3). The right column**
 259 **displays the GEOS-Chem model simulations along the respective flight tracks of each campaign (panels b and d). All data**
 260 **are averaged over 1 km vertical bins.**

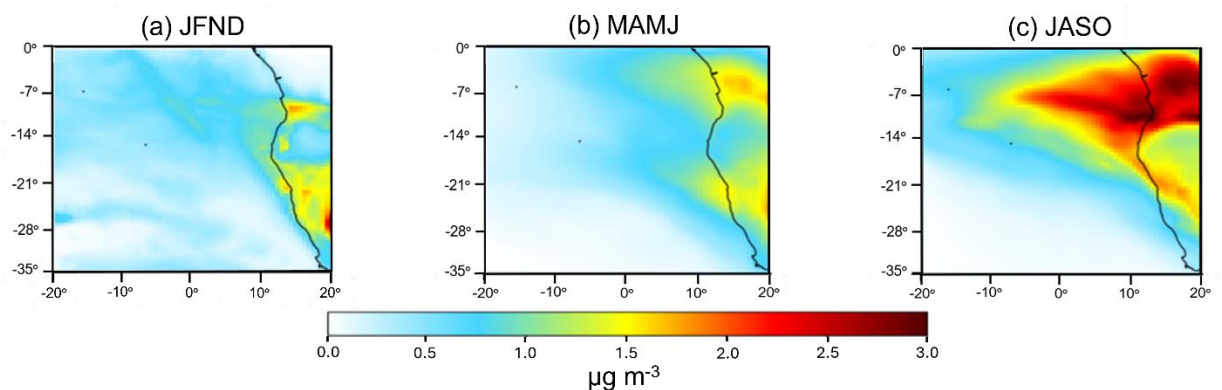
261 At altitudes where clouds persist in the domain (0 to 2 km), sulfate and organic aerosols are the dominant aerosol
 262 types. Here, the model effectively captures the mass concentration of organic aerosols, with an NMB ranging from -
 263 0.40% for ORACLES to -14% for CLARIFY. However, it underestimates sulfate aerosol concentrations by 19% at
 264 cloud altitudes for both campaigns. For other aerosol types and altitudes, the model consistently underestimates
 265 concentrations, except for sulfate and ammonium aerosols between 2 to 4 km during the ORACLES campaign, which
 266 the model overestimates by 40% and 4.6%, respectively. The model captures the total aerosol mass from 0 through 7
 267 km for sulfate and ammonium aerosols during the ORACLES campaign, with only minimal underestimations of 1.5%
 268 and 0.7%, respectively. This indicates a potential discrepancy in the vertical distribution of these aerosols rather than
 269 in total mass.

270 **3.2 Seasonal variation in aerosol composition and sources at cloud altitudes**



271
 272 **Figure 6: Simulated mean fractional aerosol composition at cloud heights (0–2 km) over the ocean in the stratocumulus**
 273 **sub-domain (0–35° S, 20° E–20° W) by season: (a) JFND, (b) MAMJ, and (c) JASO. Here SO₄, NH₄, NO₃, BC, TOA, SSA**
 274 **represents sulfate, ammonium, nitrate, black carbon, total organic aerosol and accumulation-mode sea salt aerosols,**
 275 **respectively.**

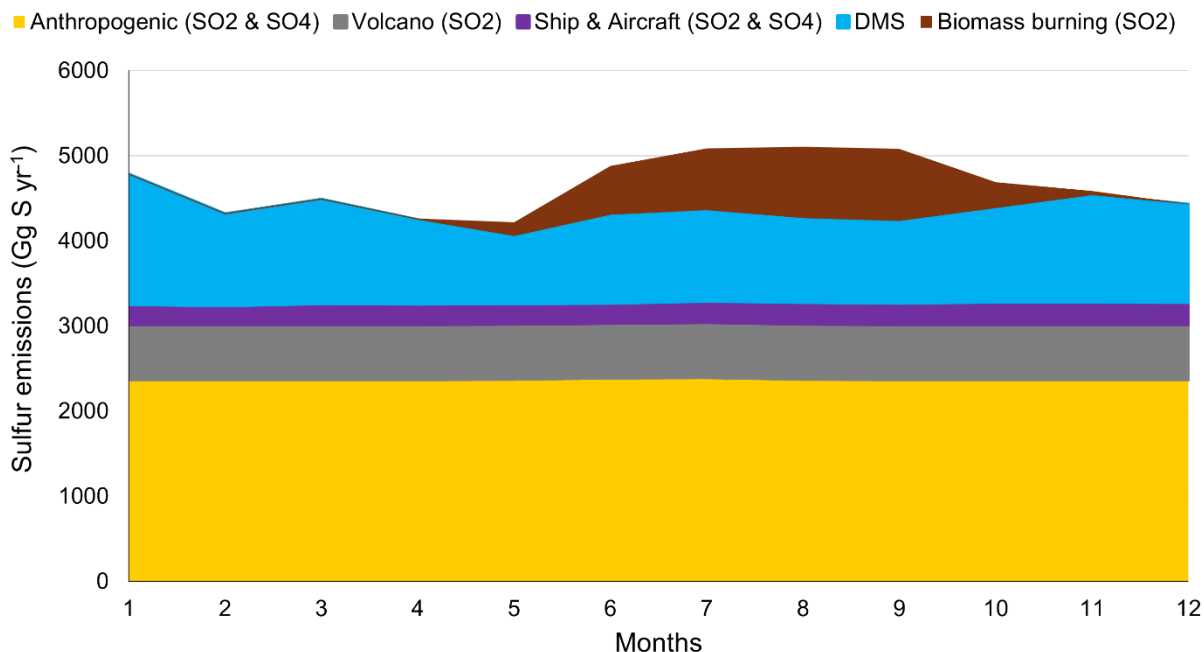
276 Figure 6 presents the simulated seasonal mean aerosol fractional composition within cloud-relevant altitudes (0–2 km),
 277 averaged over the ocean only across the subdomain (0–35° S, 20° E – 20° W) (see the map shown in Fig. 7). This area
 278 is strategically selected to coincide with the persistent Sc cloud deck and enhance our analysis of aerosol-cloud
 279 interactions. Organic aerosols, an indicator of biomass burning, predominate during both the biomass burning (JASO)
 280 and transitional (MAMJ) periods. In contrast, sulfate aerosols dominate during austral summer, likely influenced by
 281 the high primary production from coastal upwelling that leads to DMS emissions. We investigate the model
 282 representation of sulfate and these processes further in subsequent sections. An increase in the accumulation-mode
 283 sea-salt aerosols (radius 0.01–0.5 μm) contribution (total mass of 6.7 Gg) is observed in summer (Fig. 6a) as well,
 284 compared to other seasons (5.2 Gg during MAMJ and 5.8 Gg during JASO), owing to the peak wind speeds in the
 285 southern Benguela region in this season (Hutchings et al., 2009). Black carbon, ammonium, and nitrate aerosols make
 286 minor contributions to simulated aerosol mass at cloud height throughout the year.



288 **Figure 7: Spatial distribution of simulated mean sulfate aerosol concentrations averaged over cloud altitudes (0–2 km) in**
 289 **the sub-domain (0–35° S, 20° E–20° W) by season in 2017: (a) peak DMS emission season (JFND), (b) transitional phase**
 290 **(MAMJ), and (c) biomass burning season (JASO).**

291 **3.2.1 Drivers of sulfate aerosol and importance of marine precursor emissions**

292 Sulfate aerosols are the most or 2nd most important aerosol component in cloud heights over the SEA (Fig. 6). We
 293 examine the sources of sulfur emissions within the model in Figure 8. Within the broader domain (0–40° S, 40° E–
 294 20° W), anthropogenic activities are the largest source of sulfur emissions throughout the year (Fig. 8). However, the
 295 model default CEDS inventory (Hoesly et al., 2018) fails to capture the seasonality of these emissions due to absence
 296 of regional inventories and reliance on the global datasets such as the International Energy Agency (IEA) energy
 297 statistics. The anthropogenic emissions are followed by DMS emissions from the ocean, which become more
 298 pronounced during the austral summer, peaking in January. Additionally, biomass burning contributes to SO₂
 299 emissions seasonally, becoming the 3rd most important source of total sulfur emissions during July - September (Fig.
 300 8). In contrast, sulfur contributions from volcanic, shipping, and aircraft emissions remain minimal and constant year-
 301 round, reflecting assumptions of static fuel burned and emission levels across inventories.

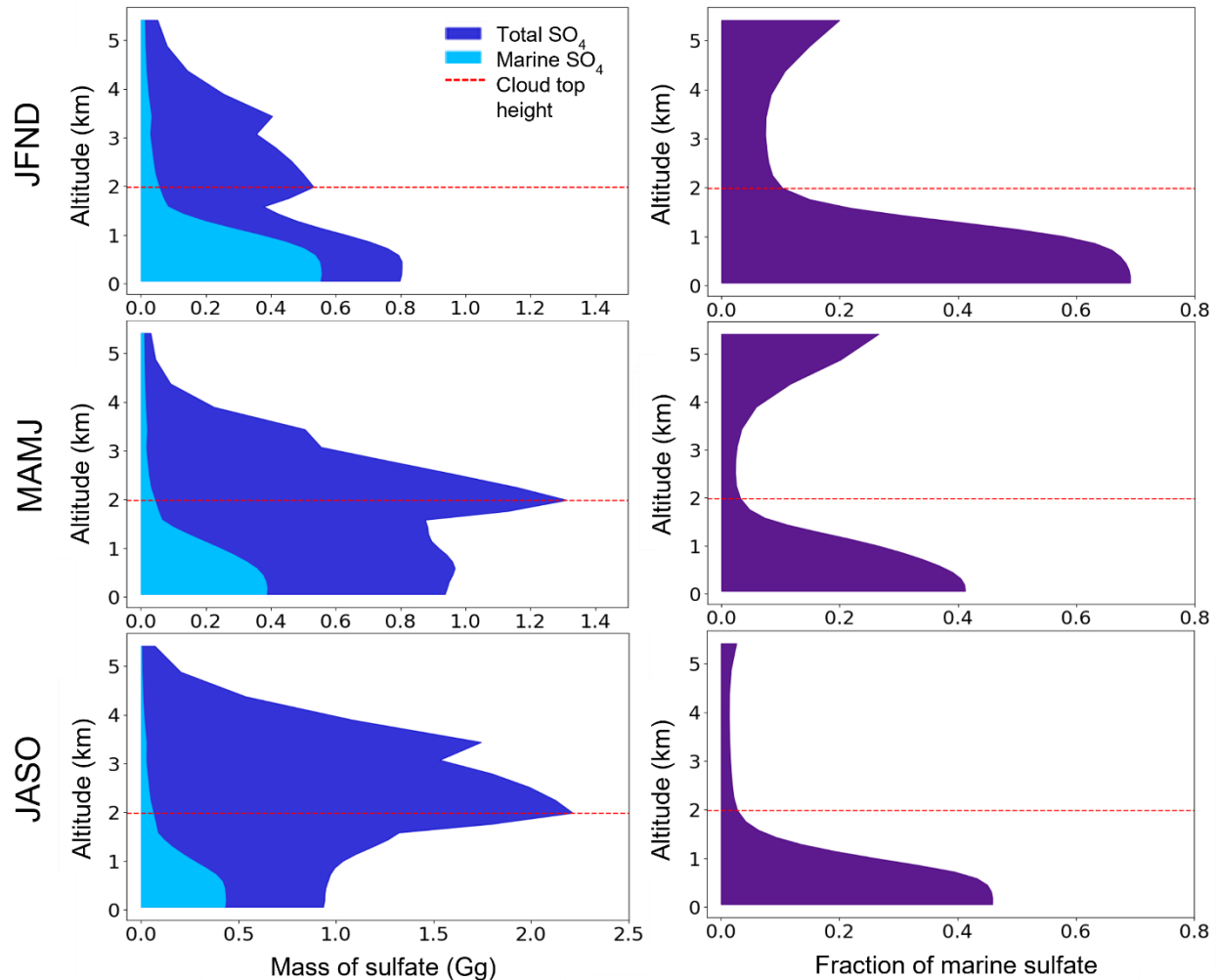


302 **Figure 8: Stacked area chart of monthly total sulfur emissions by source for 2017 across the study domain (0–40° S,**
 303 **40° E–20° W) in gigagrams of sulfur per year (Gg S yr⁻¹). Sources are indicated by color and encompass anthropogenic**
 304 **activities, volcanic activity, ship and aircraft emissions, biomass burning and natural emissions of dimethyl sulfide**
 305 **(DMS).**

307 To improve understanding of the processes driving sulfate aerosol concentrations in the region, we examine its
 308 simulated spatial distribution averaged by season over the cloud height (0–2 km) in Fig. 7. Elevated concentrations of
 309 DMS, resulting from higher rates of primary production (Lana et al., 2011; Galí et al., 2018), lead to an increase in

310 sulfate concentrations along the coastline of the Benguela region and the inner shelf of Namibia during JNFD (Fig.
311 7a), aligning with the AOD hotspot observed in Fig. 3a. This is consistent with the simulated dominance of sulfate
312 aerosols at cloud-relevant altitudes during JFND (Fig. 6a). During the biomass burning months (JASO), while their
313 relative contribution decreases (Fig. 6c), sulfate aerosols display a pronounced increase in absolute concentration (Fig.
314 7c) as a consequence of savanna fire emissions from southwestern Africa (van der Werf et al., 2010; Das et al., 2017).
315 As outlined in the AOD evaluation (Sect. 3.1.1), the model underestimates the transport of emissions to remote sites
316 (Fig A1), resulting in a steep gradient in sulfate concentrations from the eastern landmass towards the western open
317 ocean.

318 To quantitatively estimate the contribution of marine precursor emissions to sulfate aerosols, we compare the sulfate
319 mass between the standard and marine emissions only sensitivity simulations (Sect. 2.1). Figure 9 shows seasonally
320 averaged vertical profiles over the ocean region of the Sc sub-domain (0° – 35° S, 20° E– 20° W). The figure presents
321 the marine-only sulfate mass and the total sulfate mass from the standard simulation (left panels), and the ratio of
322 marine sulfate to total sulfate (right panels). Vertical profiles were computed by summing the sulfate mass within each
323 grid box, scaled by the grid box ocean fraction, across latitude and longitude within each vertical layer of the model,
324 and then averaged temporally across each season.



325

326 **Figure 9: Simulated vertical profiles of sulfate aerosol mass over oceanic regions within the sub-domain (0°–35° S, 20° E–**
 327 **20° W) by season. The left panel shows the mass of total and marine sulfate aerosols, and the right panel indicates the sulfate**
 328 **fraction from marine sources. The top row corresponds to the peak dimethyl sulfide (DMS) emission period (JFND); the**
 329 **middle row to the transitional period (MAMJ); and the bottom row to the peak biomass burning period (JASO) (note: the**
 330 **bottom left panel displays a higher x-axis scale). The upper red dashed line denotes the typical maximum cloud top height**
 331 **(Redemann et al., 2021).**

332 Our analysis highlights the substantial influence of marine sulfur sources on sulfate during JFND, as evidenced in the
 333 top left panel of Fig. 9. During this period the proportion of marine sulfate reaches up to 69.1% within-cloud (from
 334 surface to 2 km). The contribution of marine sulfate within the cloud in the subsequent periods is reduced (ranging
 335 between 2.7–45.9%; Fig. 9). We find that marine-sourced sulfate mass remains fairly consistent throughout the year
 336 (Fig. 9, left panels), with variations in the marine sulfate fraction (Fig. 9, right panels) mainly due to changes in land-
 337 based sulfate sources. Total sulfate mass during seasons influenced by biomass burning (MAMJ and JASO) peaks at
 338 2 km, with greater mass above 2 km during peak biomass burning (JASO) in contrast to JFND where mass peaks
 339 within clouds (0–2 km).

340 Table 3 summarizes the monthly mean percent contribution of marine sulfate averaged across cloud altitudes (0–2
 341 km). The annual average total sulfate mass and marine sulfate mass is 16.2 Gg and 3.5 Gg, respectively. The within-
 342 cloud marine sulfate contribution peaks in January (57.7%) and is smallest in September (10.3%). Thus, our analysis
 343 suggests that DMS emissions influence sulfate aerosol formation and their interactions with clouds in the region
 344 throughout most of the year, excepting only the peak biomass burning season. This emphasizes that constraining
 345 marine sulfur sources and chemistry both in chemical transport and climate models may improve representation of
 346 aerosol-climate dynamics in the SEA region. Limited available observations suggest the model is biased low in AOD
 347 throughout most of the year (Sect. 3.1.1), and underestimates sulfate aerosol concentrations in August and September
 348 at cloud altitudes (Sect. 3.1.2, Fig. 5). We explore related uncertainties and their implications in the following
 349 sections.

350 **Table 3:** Seasonal variation of percentage of monthly mean percent contribution of marine sulfate within cloud
 351 height

Month	Percentage of marine sulfate
January	57.7
February	54.8
March	25.3
April	26.6
May	15.3
June	15.0
July	14.8
August	14.7
September	10.3
October	22.4
November	39.1
December	44.3

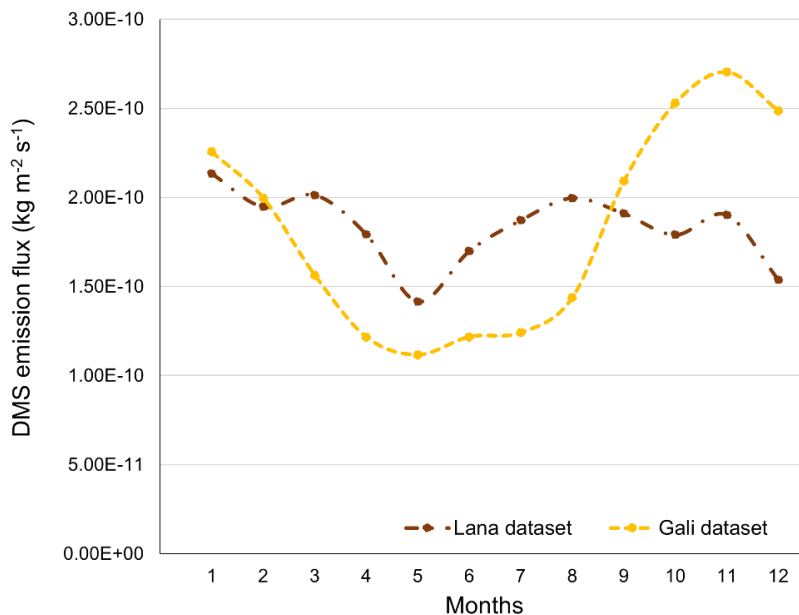
352

353 **3.3 Uncertainties**

354 **3.3.1 Assessing variations in DMS emission rates and oxidation mechanism on sulfate aerosol formation**

355 The Benguela region has substantial uncertainties in DMS concentrations in surface seawater (Asher et al., 2011;
356 Tortell et al., 2011) and the corresponding emission fluxes owing to the limited availability of biogenic sulfur
357 measurements. To investigate the sensitivity of DMS emission fluxes to changes in surface seawater DMS
358 concentrations, we conducted two simulations with DMS concentrations from Lana et al. (2011) and Galí et al. (2018)
359 (see Sect. 2.1). The standard results presented thus far were conducted using the Lana dataset.

360 In the southern Benguela, south of approximately 27° S, marked upwelling during the austral summer (Shannon and
361 Nelson, 1996; Hutchings et al., 2009) promotes phytoplankton growth and elevates DMS emissions. Figure 10
362 indicates that the Lana dataset aligns with this phenomenon, displaying peak DMS emission fluxes over the Sc sub-
363 domain in January. However, it lacks clear seasonality for the remaining months. In contrast, satellite-based DMS
364 estimates from Galí show pronounced emissions throughout the austral summer (JFND), as shown in Fig. 10. Both
365 datasets concur in magnitude for January and February, a period with better data coverage in the Lana et al. (2011)
366 climatological data set over the domain. However, the Lana dataset DMS emissions are up to 38% less during
367 December, while 51% higher in July relative to the Galí dataset. This suggests the marine contribution to sulfate in
368 our standard simulation using the Lana dataset may be underestimated from October through December
369 (encompassing two months of the peak DMS season) and overestimated from March through August (Fig. 10).



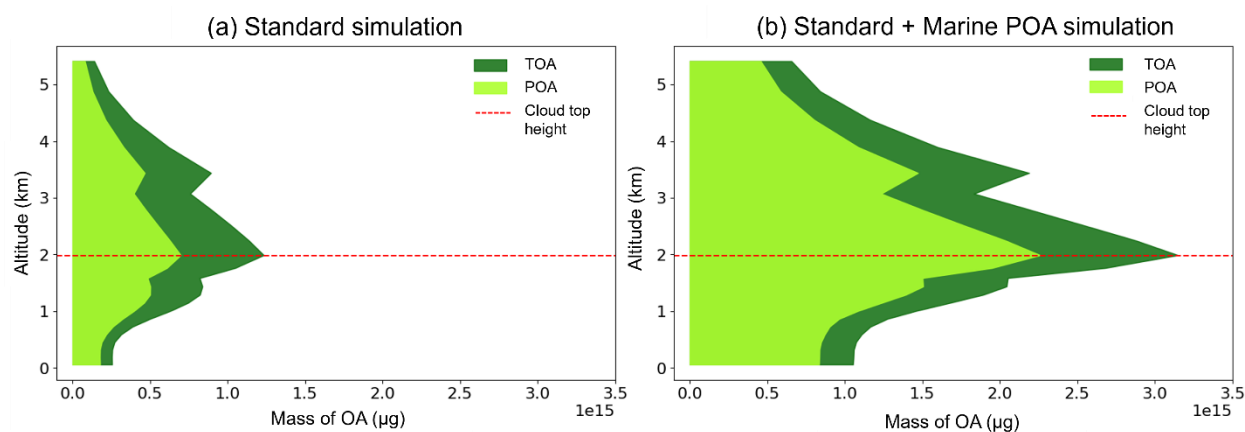
370
371 **Figure 10:** Monthly DMS emissions over the stratocumulus sub-domain (0–35° S, 20° E–20° W) using two distinct
372 datasets for surface seawater DMS concentrations. The brown dashed line presents emissions calculated using Lana

373 et al. (2011) climatology, which compiles data across 1972-2009 from multiple sources. In contrast, the yellow dashed
374 line depicts emissions based on satellite-derived estimates of surface seawater DMS concentrations (Galí et al., 2018).

375 The ongoing discovery of complexities within DMS oxidation mechanisms, along with the incomplete incorporation
376 of these mechanisms into atmospheric chemistry models, further contributes to uncertainties in predicting the impact
377 of DMS emissions on aerosols and climate (Faloona, 2009; Quinn and Bates, 2011; Carslaw et al., 2013). Chen et al.
378 (2018) highlighted the impacts of changes to DMS chemistry in the GEOS-Chem model, integrating a series of
379 multiphase sulfur oxidation mechanisms and two DMS intermediates, which led to a decrease in the global DMS
380 burden, thereby decreasing SO_2 and sulfate levels. On the other hand, Novak et al. (2021) found that the cloud uptake
381 of hydroperoxymethyl thioformate (HPMTF), a newly identified oxidation product of DMS (Wu et al., 2015; Veres
382 et al., 2020), lowers near-surface SO_2 concentration while elevating sulfate concentration in the model. Most recently,
383 Tashmim et al. (2024) implemented an advanced DMS oxidation mechanism in GEOS-Chem that incorporates the
384 latest developments in DMS chemistry, including those previously mentioned, which led to a lower SO_2 mixing ratio
385 ($\sim 70\%$) and a higher SO_4 mixing ratio ($\sim 35\%$) over the SEA during austral summer. Thus, an improved representation
386 of DMS emissions and oxidation chemistry in the model could enhance the sulfate aerosol estimations during the peak
387 DMS season. This refinement may address model underestimates of aerosol concentrations during this period (Sect.
388 3.1.1).

389 3.3.2 Exploring the impact of marine organic aerosol emissions on organic aerosol concentrations

390 Beyond marine sulfate and sea-salt aerosols, organic matter also makes a significant contribution to marine aerosol
391 mass (Middlebrook et al., 1998; Oppo et al., 1999; Russell et al., 2010). Notably, substantial concentrations of organic
392 carbon aerosols have been observed in marine regions, particularly during periods of intense biological activity
393 (O'Dowd et al., 2004). These aerosols can also increase CCN, affecting cloud properties and radiative balance (Arnold
394 et al., 2009; Gantt and Meskhidze, 2013). However, the standard GEOS-Chem model does not account for these
395 marine organic aerosol emissions. Here, we analyzed the impact of marine POA on cloud-altitude aerosols over the
396 SEA by incorporating marine POA emissions based on satellite-derived chlorophyll-a concentrations (Gantt et al.,
397 2015; See Sect. 2.1) in the model.



398

399 **Figure 11: Vertical distribution of organic aerosol mass during November 2017, the month of maximum discrepancy**
400 **between the standard and MPOA simulations, over the Sc sub-domain (0–35° S, 20° E–20° W). Left: mass profile for total**
401 **organic aerosols (TOA) and primary organic aerosols (POA) under standard simulation conditions (Std); right: when**
402 **marine primary organic aerosol (MPOA) emissions are included (Std + MPOA). The red dashed line indicates the typical**
403 **maximum cloud top height.**

404 We find that the inclusion of MPOA emissions consistently resulted in higher organic aerosol mass, with the greatest
405 increase in November. Figure 11 shows the vertical distribution of total organic aerosols (TOA) mass and POA mass
406 (including MPOA and other POA sources) with and without MPOA emissions during this month. Similar to our earlier
407 vertical profile analysis (refer to Sect. 3.2.2), we find that the maximum organic aerosol mass occurred at the highest
408 cloud top height (2 km). The Standard + MPOA simulated peak total organic aerosol mass was approximately three
409 times higher than that in the Standard simulation, highlighting the potential contribution of marine sources to total
410 organic aerosol mass concentrations. However, during the biomass burning season, the sensitivity simulation showed
411 only a minimal increase, indicating that it does not adequately address the model’s underestimation (refer to Fig. 5).
412 Gantt et al. (2015) demonstrated that including MPOA emissions in GEOS-Chem reduced the normalized mean bias
413 (NMB) of surface organic aerosol concentrations at coastal sites by 67%. Additionally, Pai et al. (2020) noted that
414 without a marine POA source, the model fails to accurately reproduce lower-tropospheric concentrations over oceans,
415 although the marine POA scheme might be biased high. Despite the limitations of a chlorophyll-based
416 parameterization like the one used here in providing mechanistic understanding of the seasonal and geographical
417 variability of organic matter emissions from sea spray (Burrows et al., 2022), our findings suggest that MPOA may
418 play a role in aerosol-cloud interactions outside of the biomass burning season, in addition to marine-derived sulfate
419 from DMS (Sect. 3.2).

420 **3.3.3 Impacts of uncertainties in biomass burning emissions of SO₂**

421 To assess the impact of uncertainty in biomass burning emissions of SO₂ on the relative contribution of marine vs.
422 land sources to aerosol, we performed a sensitivity analysis using two alternative inventories, QFED and GFAS (see
423 Sect. 2.1 and Fig. A3). The standard simulations, as detailed in Sect. 2.3, use the default biomass burning inventory
424 in GEOS-Chem, GFED. The GFAS inventory SO₂ and CO emissions over the domain are constant in time, aligning
425 with QFED during the non-biomass burning months (Fig. A3). We find that CO emissions from GFED and QFED
426 align closely; however, there is a notable difference in SO₂ emissions between the two inventories (Fig. A3). These
427 discrepancies likely originate from variations in SO₂ emission factors employed by each inventory. In July, which
428 exhibits the largest difference between the two inventories, peak SO₂ emissions in QFED are almost five-fold higher
429 than those in GFED. This discrepancy leads to a 25% increase in sulfate aerosol concentrations at cloud altitudes
430 relative to the standard results using GFED (not shown). Consequently, the contribution of marine sulfate to total
431 sulfate (see Sect. 3.2.1) may further decrease during the peak biomass burning season if QFED is used, highlighting
432 the sensitivity of aerosol source attributions to the selected biomass burning inventory.

433 **4 Implications**

434 In this study, monthly marine sulfate constitutes between 10.3% and 57.7% of total sulfate within the cloud height,
435 peaking during the high DMS emission period. However, the default Lana et al. (2011) climatology largely
436 underestimates DMS emissions during the austral summer (November and December) by up to 38%, compared to the
437 satellite-derived estimates from Galí et al. (2018). Moreover, improvement of DMS chemistry in the model by
438 incorporating new oxidation mechanisms and intermediate products could shift the balance towards increased sulfate
439 aerosol production (with Tashmim et al., 2024 suggesting an increase of up to 35% over the SEA). Marine primary
440 organic aerosol emissions may also contribute substantially to the organic aerosol mass during the peak primary
441 production period (JNFD), highlighting the importance of marine contributions to overall aerosol concentrations.
442 Meanwhile, discrepancies in SO₂ emissions from biomass burning can increase sulfate aerosol from biomass burning
443 by up to 25%. These changes would improve the model underestimate of AOD relative to AERONET observations;
444 however, observations of aerosol composition outside of August-September are very limited and this is a large gap.
445 Our results suggest marine-sourced sulfate and organics significantly influence aerosol loading and composition in
446 the SEA, particularly during the non-biomass burning period. Accurately characterizing the seasonal dynamics of
447 aerosols within cloud heights is imperative for quantifying aerosol-cloud interactions and understanding the dynamics
448 of marine aerosols in the SEA region, where uncertainties in aerosol radiative forcing are most pronounced. This
449 understanding is essential for improving the reliability of climate models in areas critical to both regional and global
450 climate dynamics.

451 **5 Conclusion**

452 Aerosols over the southeast Atlantic strongly influence global climate dynamics due to the presence of persistent
453 stratocumulus clouds and large uncertainties in aerosol-cloud interactions. However, precisely representing these
454 interactions in global climate models remains challenging, in part due to sparse available observations, especially
455 outside of the biomass burning season. In this study, we employed the GEOS-Chem chemical transport model to
456 assess the aerosol composition at cloud-relevant altitudes (0–2 km) and identify the sensitivities to marine emissions
457 and chemistry in the southeast Atlantic. This analysis aims to enhance our understanding of the role of marine aerosols
458 and the associated uncertainties affecting aerosol-cloud interactions within this climate-sensitive region.

459 We performed nested grid simulations with a 0.5° x 0.625° horizontal resolution and evaluated the model against
460 ground-based and aircraft campaign observations throughout 2017. We analyzed results for three seasonal periods
461 with distinct dominant processes including (a) the high DMS emission season (JFND), (b) the peak biomass burning
462 season (JASO), and (c) the transitional season (MAMJ). Our analysis showed that simulated monthly average aerosol
463 optical depth (AOD) exhibits the strongest correlation ($R = 0.901$) with the AERONET AOD observations during the
464 JASO season. However, the model generally underestimates AOD throughout the year, except in the JFND period,
465 where an overestimate at Gobabeb site offset underestimations at other sites. Moreover, a comparison of aerosol
466 speciation measured at Ascension Island during the LASIC campaign indicates that the model consistently
467 underestimates sulfate aerosols. We further evaluated the simulated vertical profile of aerosol mass concentrations
468 and composition against measurements from the ORACLES and CLARIFY campaigns. These comparisons showed
469 that sulfate aerosols were underestimated by 19% at cloud-relevant altitudes of 0–2 km by both campaigns. The

470 underestimate of sulfate aerosols at lower altitudes (0-2 km), coupled with an underestimate of other aerosols at higher
471 altitudes (4-8 km), likely contributes to the overall low bias in modeled AOD. The misrepresentation of natural aerosol
472 emissions and transatlantic aerosol transport may be responsible for these underestimates. Nevertheless, discrepancies
473 increase with altitude, reflecting challenges in accurately modeling high-altitude aerosol concentrations.

474 Analysis of seasonal mean aerosol composition at cloud height showed that organic aerosols predominate during
475 JASO (63%) and MAMJ (51%), while sulfate aerosols are most prevalent (41%) during the austral summer (JFND).
476 Given the prominence of sulfate as a marine sourced aerosol in remote oceanic environments, we investigated the
477 processes influencing the sulfate aerosol concentrations in our domain. Throughout the year, anthropogenic sources
478 and oceanic DMS emissions are the primary atmospheric sulfur contributors. Spatial mapping across the sub-domain
479 (0–35° S, 20° E–20° W) showed high sulfate concentrations (up to $3\mu\text{g m}^{-3}$) at cloud height during the peak biomass
480 burning season (JASO), primarily from savannah fires in southern Africa. Despite this, sulfate aerosols only account
481 for 18% of the total aerosol mass in JASO.

482 Sulfate, primarily from marine sources, is the dominant aerosol at cloud-relevant altitudes during JFND in the model
483 (up to 69% marine contribution); however, significant uncertainties regarding the treatment of DMS persist that may
484 affect this finding. To assess the impact of these uncertainties on sulfate aerosols, we compared DMS emission fluxes
485 from Lana et al. (2011) climatological data, which has limited spatial and temporal coverage in our domain, with those
486 from Galí et al. (2018), which are based on satellite-based estimates of surface seawater DMS concentrations. We find
487 that, within our domain, the Lana dataset emissions estimates are 51% higher in July and 38% lower in December
488 compared to the Galí dataset. Moreover, improvement of DMS chemistry in the model by incorporating new oxidation
489 mechanisms and intermediate products could shift the balance towards increased sulfate aerosol production (with
490 Tashmim et al., 2024 suggesting an increase of up to 35% over the SEA). Additionally, emissions of marine primary
491 organic aerosols during the peak primary production period (JNFD) may substantially contribute to the mass of organic
492 aerosols which can also act as CCN. This emphasizes the critical role of marine sources in influencing aerosol
493 concentrations, even in oceanic regions impacted by large seasonal biomass burning. Variations in SO_2 emissions
494 from biomass burning could potentially increase sulfate aerosol concentrations at cloud altitudes by up to 25%.
495 Addressing these discrepancies is essential for improving the model's underestimation of AOD and aerosol
496 concentrations compared to observations.

497 This study highlights the importance of constraining marine emissions and their chemical transformations by
498 incorporating satellite-retrieved datasets and extending field campaign efforts during non-biomass burning periods.
499 Such initiatives are essential to accurately characterize seasonal aerosol dynamics at cloud heights and to improve our
500 understanding of aerosol-cloud interactions in regions with persistent low-altitude clouds. These advancements could
501 substantially minimize uncertainties in model estimates of radiative forcing and enhance the reliability of climate
502 model projections in the southeast Atlantic region.

503

504 **Appendix A**505 **Table A1:** Configuration of sensitivity analysis simulations

Simulations	Resolution	Emission inventories (References)
Marine sulfur emissions only	0.5° x 0.625°	Standard model inventories (see Section 2.1 in the main text)
DMS emissions	4° x 5°	Climatological product for seawater DMS (Lana et al., 2011); Satellite-derived DMS estimates (Galí et al., 2018)
Biomass burning inventories	4° x 5°	Global Fire Emissions Database (van der Werf et al., 2017); Quick Fire Emissions Dataset (Darmenov & da Silva, 2013); Global Fire Assimilation System (Kaiser et al., 2012).
Marine primary organics	0.5° x 0.625°	Marine primary organic aerosol emission estimates from satellite-derived chlorophyll-a concentrations (Gantt et al., 2015)

506

507

508

509

510

511

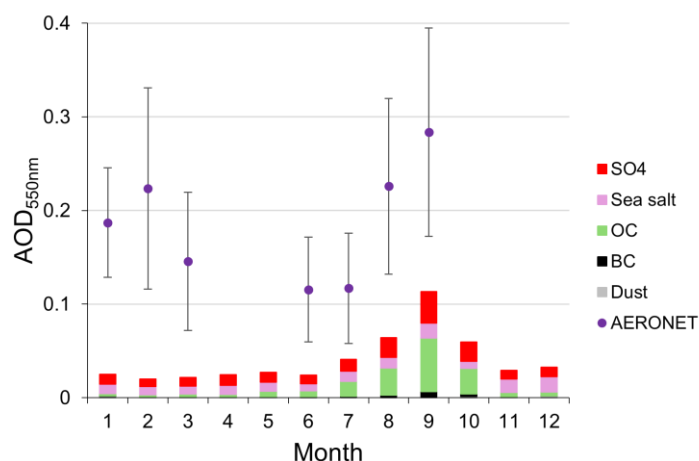
512

513

514 **Table A2:** AERONET site information and the monthly average AOD₅₅₀ value (± 1 standard deviation) for three
 515 distinct time periods per site are shown. An asterisk (first column) indicates that the mean AOD during the biomass
 516 burning season (JASO) at these sites is more than 1 standard deviation higher than the mean AOD in other season(s)
 517 (JFND and MAMJ).

Site	Latitude (°)	Longitude (°)	Months of data availability for 2017	Monthly Average AOD _{550nm} ± 1 SD (JFND)	Monthly Average AOD _{550nm} ± 1 SD (MAMJ)	Monthly Average AOD _{550nm} ± 1 SD (JASO)
Ascension Island	-7.976	-14.415	7	0.320 \pm 0.061	0.256 \pm 0.046	0.396 \pm 0.078
Gobabeb	-23.562	15.041	12	0.268 \pm 0.033	0.254 \pm 0.032	0.399 \pm 0.115
HESS*	-23.273	16.503	10	0.162 \pm 0.024	0.211 \pm 0.033	0.368 \pm 0.108
Henties_Bay*	-22.095	14.26	3	0.166 \pm 0.021	0.138 \pm 0.021	0.380 \pm 0.114
Lubango*	-14.958	13.445	9	0.120 \pm 0.011	0.251 \pm 0.011	0.534 \pm 0.139
Namibe*	-15.159	12.178	8	0.279 \pm 0.028	0.314 \pm 0.029	0.689 \pm 0.192
Simonstown_IMT*	-34.193	18.446	7	0.246 \pm 0.049	0.179 \pm 0.018	N/A
Upington	-28.379	21.156	8	0.131 \pm 0.019	0.193 \pm 0.035	0.321 \pm 0.115
Windport*	-19.366	15.483	10	0.249 \pm 0.041	0.242 \pm 0.037	0.514 \pm 0.159

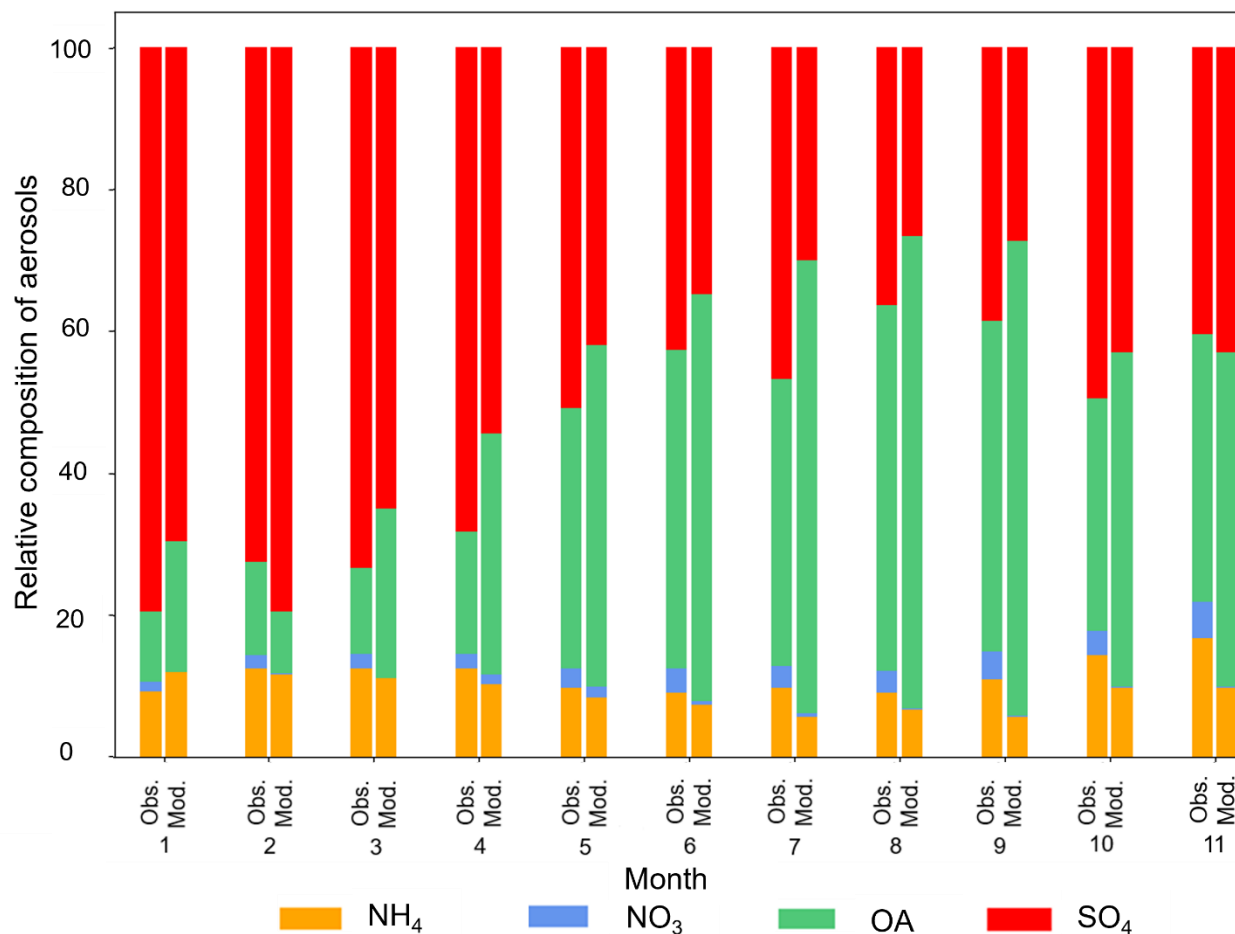
518



519

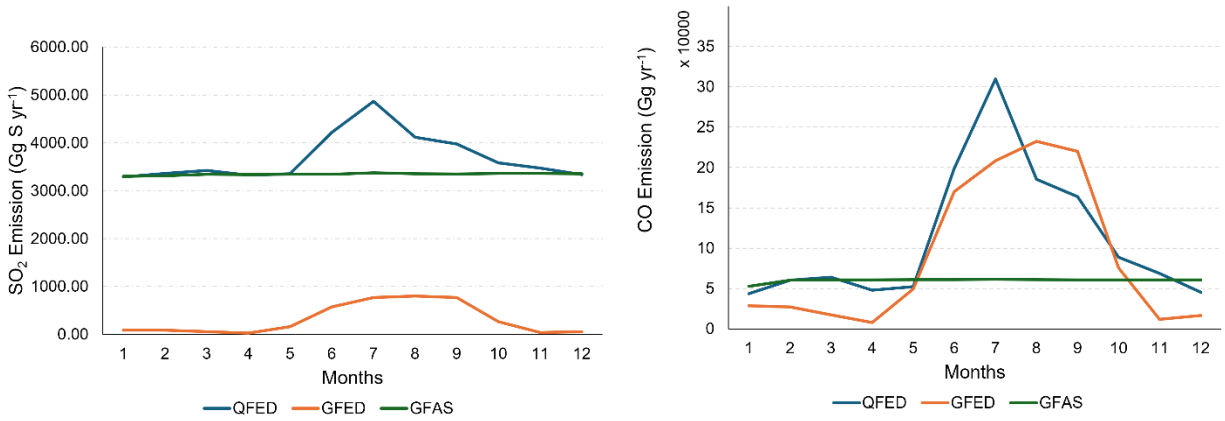
520 **Figure A1:** Comparative analysis of aerosol optical depth at 550 nm (AOD_{550nm}) for Ascension Island in 2017. The
 521 purple dots present the measured mean monthly AOD values, with vertical error bars illustrating the range of AOD_{550nm}
 522 measurements captured by the AERONET ground station. The stacked bars represent the GEOS-Chem model's

523 simulated AOD values, with each layer corresponding to the major aerosol components, such as sulfate (SO₄), sea
 524 salt, organic carbon (OC), black carbon (BC), and dust, providing insight into the model's aerosol composition
 525 representation.



526
 527 **Figure A2:** Comparative analysis of the relative aerosol composition at Ascension Island in 2017. The stacked bars
 528 on the left depict observations of chemical composition taken during the LASIC campaign at the ARM facility on
 529 Ascension Island, utilizing an aerosol chemical speciation monitor (ACSM) at 341 meters. The bars on the right
 530 illustrate the GEOS-Chem simulated aerosol composition at the same coordinates. Each segment of the stack
 531 represents different aerosol components: ammonium (NH₄), nitrates (NO₃), organic aerosols (OA), and sulfate (SO₄).

532
 533
 534
 535
 536



537

538 **Figure A3:** Comparison of biomass burning emissions across various inventories, namely GFED, QFED, and GFAS
 539 across the domain (0–40° S, 40° E–20° W). The panels depict the interannual variability of biomass burning emissions,
 540 with the left panel illustrating sulfur dioxide (SO₂) emissions, and the right panel displaying carbon monoxide (CO)
 541 emissions. Both GFED and QFED indicate similar emission trends; however, GFED exhibits lower SO₂ emission
 542 magnitudes compared to QFED. GFAS presents emission magnitudes similar to QFED during non-biomass burning
 543 period.

Code and data availability

The GEOS-Chem model used here is publicly available at <https://zenodo.org/records/5748260>. The ORACLES campaign data from 2017 are available at: https://doi.org/10.5067/Suborbital/ORACLES/P3/2017_V2 (last access January 26, 2024). The CLARIFY campaign data are available at <https://catalogue.ceda.ac.uk/uuid/38ab7089781a4560b067dd6c20af3769> (last access February 12, 2024). The ACSM dataset from LASIC campaign is available at <https://doi.org/10.5439/1763029> (last access September 10, 2024).

Author contributions

MH, HMM, and RMG designed the research. MH conducted the model simulations, analysis, and visualization, with expert advice from HMM. MH drafted the manuscript, which was then revised by all co-authors.

Competing interests

At least one of the (co-)authors is a member of the editorial board of Atmospheric Chemistry and Physics.

Acknowledgements

Mashiat Hossain and Hannah M. Horowitz gratefully acknowledge Michael Diamond for discussions on cloud-relevant altitudes over the southeast Atlantic region.

References

- Adebiyi, A. A., and Zuidema, P.: The role of the southern African easterly jet in modifying the southeast Atlantic aerosol and cloud environments, *Q. J. Roy.*, 142, <https://doi.org/10.1002/qj.2765>, 2016.
- Adebiyi, A. A., Zuidema, P., and Abel, S. J.: The convolution of dynamics and moisture with the presence of shortwave absorbing aerosols over the southeast Atlantic, *JCLI*, 28, <https://doi.org/10.1175/JCLI-D-14-00352.1>, 2015.
- Adebiyi, A. A., Akinsanola, A. A., and Ajoku, O. F.: The Misrepresentation of the Southern African Easterly Jet in Models and Its Implications for Aerosol, Clouds, and Precipitation Distributions, *JCLI*, 36, <https://doi.org/10.1175/JCLI-D-23-0083.1>, 2023.
- Alexander, B., Park, R. J., Jacob, D. J., and Gong, S.: Transition metal-catalyzed oxidation of atmospheric sulfur: Global implications for the sulfur budget. *J. Geophys. Res.*, 114, <https://doi.org/10.1029/2008JD010486>, 2009.
- Andreae, M. O.: Ocean-atmosphere interactions in the global biogeochemical sulfur cycle, *Mar. Chem.*, 30, [https://doi.org/10.1016/0304-4203\(90\)90059-L](https://doi.org/10.1016/0304-4203(90)90059-L), 1990.
- Andreae, M. O., Elbert, W., and De Mora, S. J.: Biogenic sulfur emissions and aerosols over the tropical South Atlantic. 3. Atmospheric dimethylsulfide, aerosols and cloud condensation nuclei, *J. Geophys. Res.*, 100, <https://doi.org/10.1029/94jd02828>, 1995.
- Arnold, S. R., Spracklen, D. V., Williams, J., Yassaa, N., Sciare, J., Bonsang, B., Gros, V., Peeken, I., Lewis, A. C., Alvain, S., and Alvain, M.: Evaluation of the global oceanic isoprene source and its impacts on marine organic carbon aerosol, *Atmos. Chem. Phys.*, 9, <https://doi.org/10.5194/acp-9-1253-2009>, 2009.

- Arowosegbe, O. O., Röösl, M., Adebayo-Ojo, T. C., Dalvie, M. A., and de Hoogh, K.: Spatial and Temporal Variations in PM₁₀ Concentrations between 2010–2017 in South Africa, *Int. J. Environ. Res. Public Health*, 18, 1–12, doi.org/10.1016/j.envpol.2022.119883, 2021.
- Asher, E.C., Merzouk, A., and Tortell, P.D.: Fine-scale spatial and temporal variability of surface water dimethylsulfide (DMS) concentrations and sea–air fluxes in the NE Subarctic Pacific, *Mar. Chem.*, 126, 63–75, <https://doi.org/10.1016/j.marchem.2011.03.009>, 2011.
- Barnes, I., Hjorth, J., and Mihalopoulos, N.: Dimethyl sulfide and dimethyl sulfoxide and their oxidation in the atmosphere, *Chem. Rev.*, 106, <https://doi.org/10.1021/cr020529>, 2006.
- Barrett, P. A., Abel, S. J., Coe, H., Crawford, I., Dobracki, A., Haywood, J., Howell, S., Jones, A., Langridge, J., McFarquhar, G. M., Nott, G. J., Price, H., Redemann, J., Shinozuka, Y., Szpek, K., Taylor, J. W., Wood, R., Wu, H., Zuidema, P., ... Zhang, J.: Intercomparison of airborne and surface-based measurements during the CLARIFY, ORACLES and LASIC field experiments, *Atmos. Meas. Tech.*, 15, 6329–6371. <https://doi.org/10.5194/amt-15-6329-2022>, 2022.
- Bates, T. S., Lamb, B. K., Guenther, A., Dignon, J., and Stoiber, R. E.: Sulfur emissions to the atmosphere from natural sources, *J. Atmos. Chem.*, 14, 1–4, <https://doi.org/10.1007/BF00115242>, 1992.
- Brooks, S. D., and Thornton, D. C. O.: Marine aerosols and clouds, *Ann. Rev. Mar. Sci.*, 10, <https://doi.org/10.1146/annurev-marine-121916-063148>, 2018.
- Burkholder, J. B., Sander, S. P., Abbatt, J., Barker, J. R., Huie, R. E., Kolb, C. E., Kurylo, M. J., Orkin, V. L., Wilmouth, D. M., and Wine, P. H.: Chemical Kinetics and Photochemical Data for Use in Atmospheric Studies, Evaluation No. 18, JPL Publication 15-10, Jet Propulsion Laboratory, Pasadena, available at: <http://jpldataeval.jpl.nasa.gov> (last access: 10 May 2024), 2015.
- Burrows, S. M., Easter, R. C., Liu, X., Ma, P. L., Wang, H., Elliott, S. M., Singh, B., Zhang, K., and Rasch, P. J.: OCEANFILMS (Organic Compounds from Ecosystems to Aerosols: Natural Films and Interfaces via Langmuir Molecular Surfactants) sea spray organic aerosol emissions - implementation in a global climate model and impacts on clouds, *Atmos. Chem. Phys.*, 22, <https://doi.org/10.5194/acp-22-5223-2022>, 2022.
- Carslaw, K. S., Lee, L. A., Reddington, C. L., Pringle, K. J., Rap, A., Forster, P. M., Mann, G. W., Spracklen, D. V., Woodhouse, M. T., Regayre, L. A., and Pierce, J. R.: Large contribution of natural aerosols to uncertainty in indirect forcing, *Nature*, 503, <https://doi.org/10.1038/nature12674>, 2013.
- Chen, H., Ezell, M. J., Arquero, K. D., Varner, M. E., Dawson, M. L., Gerber, R. B., and Finlayson-Pitts, B. J.: New particle formation and growth from methanesulfonic acid, trimethylamine and water, *Phys. Chem. Chem. Phys.*, 17, <https://doi.org/10.1039/c5cp00838g>, 2015.
- Chen, Q., Sherwen, T., Evans, M., and Alexander, B.: DMS oxidation and sulfur aerosol formation in the marine troposphere: A focus on reactive halogen and multiphase chemistry, *Atmos. Chem. Phys.*, 18, <https://doi.org/10.5194/acp-18-13617-2018>, 2018.
- Chen, Y. C., Christensen, M. W., Stephens, G. L., and Seinfeld, J. H.: Satellite-based estimate of global aerosol-cloud radiative forcing by marine warm clouds, *Nat. Geosci.*, 7, <https://doi.org/10.1038/ngeo2214>, 2014.
- Chin, M., Jacob, D. J., Gardner, G. M., Foreman-Fowler, M. S., Spiro, P. A., and Savoie, D. L.: A global three-dimensional model of tropospheric sulfate, *J. Geophys. Res.*, 101, <https://doi.org/10.1029/96jd01221>, 1996.
- Croft, B., Martin, R. V., Moore, R. H., Ziemba, L. D., Crosbie, E. C., Liu, H., Russell, L. M., Saliba, G., Wisthaler, A., Müller, M., Schiller, A., Galí, M., Chang, R. Y. W., McDuffie, E. E., Bilsback, K. R., and Pierce, J. R.: Factors controlling marine aerosol size distributions and their climate effects over the northwest Atlantic Ocean region, *Atmos. Chem. Phys.*, 21, <https://doi.org/10.5194/acp-21-1889-2021>, 2021.

Dang, C., Segal-Rozenhaimer, M., Che, H., Zhang, L., Formenti, P., Taylor, J., Dobracki, A., Purdue, S., Wong, P., Nenes, A., Sedlacek III, A., Coe, H., Redemann, J., Zuidema, P., Howell, S., and Haywood, J.: Biomass burning and marine aerosol processing over the southeast Atlantic Ocean: a TEM single-particle analysis, *Atmos. Chem. Phys.*, 22, 9389–9412, [10.5194/acp-22-9389-2022](https://doi.org/10.5194/acp-22-9389-2022), 2022.

Darmenov, A., and da Silva, A. M.: The Quick Fire Emissions Dataset (QFED) - Documentation of versions 2.1, 2.2 and 2.4. NASA Tech. Rep. Ser. Glob. Model. Data Assim. NASA TM-2013-104606, 32, 1–183, 2013.

Das, S., Harshvardhan, H., Bian, H., Chin, M., Curci, G., Protonotariou, A. P., Mielonen, T., Zhang, K., Wang, H., and Liu, X.: Biomass burning aerosol transport and vertical distribution over the South African-Atlantic region, *J. Geophys. Res.*, 122, <https://doi.org/10.1002/2016JD026421>, 2017.

Diamond, M. S., Dobracki, A., Freitag, S., Griswold, J. D. S., Heikkila, A., Howell, S. G., Kacarab, M. E., Podolske, J. R., Saide, P. E., and Wood, R.: Time-dependent entrainment of smoke presents an observational challenge for assessing aerosol-cloud interactions over the southeast Atlantic Ocean, *Atmos. Chem. Phys.*, 18, <https://doi.org/10.5194/acp-18-14623-2018>, 2018.

Doherty, S. J., Saide, P. E., Zuidema, P., Shinozuka, Y., Ferrada, G. A., Gordon, H., Mallet, M., Meyer, K., Painemal, D., Howell, S. G., Freitag, S., Dobracki, A., Podolske, J. R., Burton, S. P., Ferrare, R. A., Howes, C., Nabat, P., Carmichael, G. R., Da Silva, A., ... Redemann, J.: Modeled and observed properties related to the direct aerosol radiative effect of biomass burning aerosol over the southeastern Atlantic, *Atmos. Chem. Phys.*, 22, <https://doi.org/10.5194/acp-22-1-2022>, 2022.

Duncan Fairlie, T., Jacob, D. J., and Park, R. J.: The impact of transpacific transport of mineral dust in the United States, *Atmos. Environ.*, 41, <https://doi.org/10.1016/j.atmosenv.2006.09.048>, 2007.

Faloon, I.: Sulfur processing in the marine atmospheric boundary layer: A review and critical assessment of modeling uncertainties, *Atmos. Environ.*, 43, <https://doi.org/10.1016/j.atmosenv.2009.02.043>, 2009.

Formenti, P., Piketh, S. J., and Annegarn, H. J.: Detection of non-sea salt sulphate aerosol at a remote coastal site in South Africa: a PIXE study, *Nucl. Instr. Meth. Phys. Res. B*, 150, 332–338, [https://doi.org/10.1016/S0168-583X\(98\)01041-6](https://doi.org/10.1016/S0168-583X(98)01041-6), 1999.

Formenti, P., D'Anna, B., Flamant, C., Mallet, M., Piketh, S. J., Schepanski, K., Waquet, F., Auriol, F., Brogniez, G., Burnet, F., Chaboureau, J. P., Chauvigné, A., Chazette, P., Denjean, C., Desboeufs, K., Doussin, J. F., Elguindi, N., Feuerstein, S., Gaetani, M., ... Holben, B.: The aerosols, radiation and clouds in southern Africa field campaign in Namibia overview, illustrative observations, and way forward, *B. Am. Meteorol. Soc.*, 100, 1277–1298, <https://doi.org/10.1175/BAMS-D-17-0278.1>, 2019.

Fountoukis, C., and Nenes, A.: ISORROPIA II: a computationally efficient thermodynamic equilibrium model for K^+ - Ca^{2+} - Mg^{2+} - NH_4^+ - Na^+ - SO_4^{2-} - NO_3^- - Cl^- - H_2O aerosols, *Atmos. Chem. Phys.*, 7, 4639–4659, <https://doi.org/10.5194/acp-7-4639-2007>, 2007.

Fung, K. M., Heald, C. L., Kroll, J. H., Wang, S., Jo, D. S., Gettelman, A., Lu, Z., Liu, X., Zaveri, R. A., Apel, E. C., Blake, D. R., Jimenez, J.-L., Campuzano-Jost, P., Veres, P. R., Bates, T. S., Shilling, J. E., and Zawadowicz, M.: Exploring dimethyl sulfide (DMS) oxidation and implications for global aerosol radiative forcing, *Atmos. Chem. Phys.*, 22, 1549–1573, <https://doi.org/10.5194/acp-22-1549-2022>, 2022.

Galí, M., Lévassieur, M., Devred, E., Simó, R., and Babin, M.: Sea-surface dimethylsulfide (DMS) concentration from satellite data at global and regional scales, *BG*, 15, 3497–3519, <https://doi.org/10.5194/bg-15-3497-2018>, 2018.

Gantt, B., and Meskhidze, N.: The physical and chemical characteristics of marine primary organic aerosol: A review, *Atmos. Chem. Phys.*, 13, 3979–3996, <https://doi.org/10.5194/acp-13-3979-2013>, 2013.

- Gantt, B., Johnson, M. S., Crippa, M., Prévôt, A. S. H., and Meskhidze, N.: Implementing marine organic aerosols into the GEOS-Chem model, *Geosci. Model Dev.*, 8, 619-629, <https://doi.org/10.5194/gmd-8-619-2015>, 2015.
- Gelaro, R., McCarty, W., Suárez, M. J., Todling, R., Molod, A., Takacs, L., Randles, C. A., Darmenov, A., Bosilovich, M. G., Reichle, R., Wargan, K., Coy, L., Cullather, R., Draper, C., Akella, S., Buchard, V., Conaty, A., da Silva, A. M., Gu, W., ... Zhao, B.: The modern-era retrospective analysis for research and applications, version 2 (MERRA-2), *J. Climate*, 30, 5419–5454, <https://doi.org/10.1175/JCLI-D-16-0758.1>, 2017.
- Giles, D. M., Sinyuk, A., Sorokin, M. G., Schafer, J. S., Smirnov, A., Slutsker, I., Eck, T. F., Holben, B. N., Lewis, J. R., Campbell, J. R., Welton, E. J., Korkin, S. V., and Lyapustin, A. I.: Advancements in the Aerosol Robotic Network (AERONET) Version 3 database - Automated near-real-time quality control algorithm with improved cloud screening for Sun photometer aerosol optical depth (AOD) measurements, *Atmos. Meas. Tech.*, 12, 169-209, <https://doi.org/10.5194/amt-12-169-2019>, 2019.
- Gong, S. L.: A Parameterization of Sea-salt Aerosol Source Function for Sub- and Super-micron Particles. *Glob. Biogeochem. Cycles*, 17(4), <https://doi.org/10.1029/2003GB002079>, 2003.
- Haywood, J. M., Abel, S. J., Barrett, P. A., Bellouin, N., Blyth, A., Bower, K. N., Brooks, M., Carslaw, K., Che, H., Coe, H., Cotterell, M. I., Crawford, I., Cui, Z., Davies, N., Dingley, B., Field, P., Formenti, P., Gordon, H., De Graaf, M., ... Zuidema, P.: The CLOUD-Aerosol-Radiation Interaction and Forcing: Year 2017 (CLARIFY-2017) measurement campaign, *Atmos. Chem. Phys.*, 21, <https://doi.org/10.5194/acp-21-1049-2021>, 2021.
- Hodzic, A., Campuzano-Jost, P., Bian, H., Chin, M., Colarco, P. R., Day, D. A., Froyd, K. D., Heinold, B., Jo, D. S., Katich, J. M., Kodros, J. K., Nault, B. A., Pierce, J. R., Ray, E., Schacht, J., Schill, G. P., Schroder, J. C., Schwarz, J. P., Sueper, D. T., ... Jimenez, J. L.: Characterization of organic aerosol across the global remote troposphere: A comparison of ATom measurements and global chemistry models, *Atmos. Chem. Phys.*, 20, <https://doi.org/10.5194/acp-20-4607-2020>, 2020.
- Hoesly, R. M., Smith, S. J., Feng, L., Klimont, Z., Janssens-Maenhout, G., Pitkanen, T., Seibert, J. J., Vu, L., Andres, R. J., Bolt, R. M., Bond, T. C., Dawidowski, L., Kholod, N., Kurokawa, J. I., Li, M., Liu, L., Lu, Z., Moura, M. C. P., O'Rourke, P. R., and Zhang, Q.: Historical (1750-2014) anthropogenic emissions of reactive gases and aerosols from the Community Emissions Data System (CEDS), *Geosci. Model Dev.*, 11(1), <https://doi.org/10.5194/gmd-11-369-2018>, 2018.
- Hoffmann, E. H., Tilgner, A., Schrödner, R., Bräuer, P., Wolke, R., and Herrmann, H.: An advanced modeling study on the impacts and atmospheric implications of multiphase dimethyl sulfide chemistry, *Proc. Natl. Acad. Sci. USA*, 113, 11776–11781, <https://doi.org/10.1073/pnas.1606320113>, 2016.
- Holben, B. N., Eck, T. F., Slutsker, I., Tanré, D., Buis, J. P., Setzer, A., Vermote, E., Reagan, J. A., Kaufman, Y. J., Nakajima, T., Lavenu, F., Jankowiak, I., and Smirnov, A.: AERONET - A federated instrument network and data archive for aerosol characterization, *Remote Sens. Environ.*, 66, 1–16, [https://doi.org/10.1016/S0034-4257\(98\)00031-5](https://doi.org/10.1016/S0034-4257(98)00031-5), 1998.
- Hutchings, L., van der Lingen, C. D., Shannon, L. J., Crawford, R. J. M., Verheye, H. M. S., Bartholomae, C. H., van der Plas, A. K., Louw, D., Kreiner, A., Ostrowski, M., Fidel, Q., Barlow, R. G., Lamont, T., Coetzee, J., Shillington, F., Veitch, J., Currie, J. C., and Monteiro, P. M. S.: The Benguela Current: An ecosystem of four components, *Prog. Oceanogr.*, 83, <https://doi.org/10.1016/j.pocean.2009.07.046>, 2009.
- Jaeglé, L., Quinn, P. K., Bates, T. S., Alexander, B., and Lin, J. T.: Global distribution of sea salt aerosols: New constraints from in situ and remote sensing observations, *Atmos. Chem. Phys.*, 11, <https://doi.org/10.5194/acp-11-3137-2011>, 2011.
- Jaeglé, L., Shah, V., Thornton, J. A., Lopez-Hilfiker, F. D., Lee, B. H., McDuffie, E. E., Fibiger, D., Brown, S. S., Veres, P., Sparks, T. L., Ebben, C. J., Wooldridge, P. J., Kenagy, H. S., Cohen, R. C., Weinheimer, A. J., Campos, T. L., Montzka, D. D., Digangi, J. P., Wolfe, G. M., ... Weber, R. J.: Nitrogen Oxides Emissions, Chemistry,

Deposition, and Export Over the Northeast United States During the WINTER Aircraft Campaign, *J. Geophys. Res.-Atmos.*, 123, <https://doi.org/10.1029/2018JD029133>, 2018.

Jarre, A., Hutchings, L., Kirkman, S. P., Kreiner, A., Tchivalanga, P. C. M., Kainge, P., Uanivi, U., van der Plas, A. K., Blamey, L. K., Coetzee, J. C., Lamont, T., Samaai, T., Verheye, H. M., Yemane, D. G., Axelsen, B. E., Ostrowski, M., Stenevik, E. K., and Loeng, H.: Synthesis: Climate effects on biodiversity, abundance and distribution of marine organisms in the Benguela, *Fish. Oceanogr.*, 24, <https://doi.org/10.1111/fog.12086>, 2015.

Kaiser, J. W., Heil, A., Andreae, M. O., Benedetti, A., Chubarova, N., Jones, L., Morcrette, J.-J., Razinger, M., Schultz, M. G., Suttie, M., and van der Werf, G. R.: Biomass burning emissions estimated with a global fire assimilation system based on observed fire radiative power, *BG*, 9, 527–554, <https://doi.org/10.5194/bg-9-527-2012>, 2012.

Kaufman, Y. J., and Tanré, D.: Effect of variations in super-saturation on the formation of cloud condensation nuclei, *Nature*, 369, 45-48, <https://doi.org/10.1038/369045a0>, 1994.

Kilgour, D. B., Novak, G. A., Sauer, J. S., Moore, A. N., Dinasquet, J., Amiri, S., Franklin, E. B., Mayer, K., Winter, M., Morris, C. K., Price, T., Malfatti, F., Crocker, D. R., Lee, C., Cappa, C. D., Goldstein, A. H., Prather, K. A., and Bertram, T. H.: Marine gas-phase sulfur emissions during an induced phytoplankton bloom, *Atmos. Chem. Phys.*, 22, 1601–1613, <https://doi.org/10.5194/acp-22-1601-2022>, 2022.

Lana, A., Bell, T. G., Simó, R., Vallina, S. M., Ballabrera-Poy, J., Kettle, A. J., Dachs, J., Bopp, L., Saltzman, E. S., Stefels, J., Johnson, J. E., and Liss, P. S.: An updated climatology of surface dimethylsulfide concentrations and emission fluxes in the global ocean, *Global Biogeochem. Cy.*, 25, <https://doi.org/10.1029/2010GB003850>, 2011.

Latimer, R. N. C., and Martin, R. V.: Interpretation of measured aerosol mass scattering efficiency over North America using a chemical transport model, *Atmos. Chem. Phys.*, 19, <https://doi.org/10.5194/acp-19-2635-2019>, 2019.

Lee, G., Park, J., Jang, Y., Lee, M., Kim, K. R., Oh, J. R., Kim, D., Yi, H. Il, and Kim, T. Y.: Vertical variability of seawater DMS in the South Pacific Ocean and its implication for atmospheric and surface seawater DMS, *Chemosphere*, 78, 1063-1070, <https://doi.org/10.1016/j.chemosphere.2009.10.054>, 2010.

Lindesay, J. A., Andreae, M. O., Goldammer, J. G., Harris, G., Annegarn, H. J., Garstang, M., Scholes, R. J., and Van Wilgen, B. W.: International geosphere-biosphere programme/international global atmospheric chemistry SAFARI-92 field experiment: Background and overview, *J. Geophys. Res.*, 101, <https://doi.org/10.1029/96jd01512>, 1996.

Martínez-Lozano, J. A., Utrillas, M. P., Tena, F., and Cachorro, V. E.: The parameterisation of the atmospheric aerosol optical depth using the Ångström power law, *Sol. Energy*, 63, 303–311, [https://doi.org/10.1016/S0038-092X\(98\)00077-2](https://doi.org/10.1016/S0038-092X(98)00077-2), 1998.

Marvin, M. R., Palmer, P. I., Yao, F., Latif, M. T., and Khan, M. F.: Uncertainties from biomass burning aerosols in air quality models obscure public health impacts in Southeast Asia, *Atmos. Chem. Phys.*, 24, 3699–3715. <https://doi.org/10.5194/acp-24-3699-2024>, 2024.

Middlebrook, A. M., Murphy, D. M., and Thomson, D. S.: Observations of organic material in individual marine particles at Cape Grim during the First Aerosol Characterization Experiment (ACE 1), *J. Geophys. Res.*, 103, <https://doi.org/10.1029/97JD03719>, 1998.

Novak, G. A., Fite, C. H., Holmes, C. D., Veres, P. R., Neuman, J. A., Faloona, I., Thornton, J. A., Wolfe, G. M., Vermeuel, M. P., Jernigan, C. M., Peischl, J., Ryerson, T. B., Thompson, C. R., Bourgeois, I., Warneke, C., Gkatzelis, G. I., Coggon, M. M., Sekimoto, K., Bui, T. P., ... Bertram, T. H.: Rapid cloud removal of dimethyl sulfide oxidation products limits SO₂ and cloud condensation nuclei production in the marine atmosphere, *Proc. Natl. Acad. Sci. USA*, 118, <https://doi.org/10.1073/pnas.2110472118>, 2021.

- O'Dowd, C. D., and De Leeuw, G.: Marine aerosol production: A review of the current knowledge, *Phil. Trans. R. Soc. A.*, 365, 1753-1774, <https://doi.org/10.1098/rsta.2007.2043>, 2007.
- O'Dowd, C. D., Facchini, M. C., Cavalli, F., Ceburnis, D., Mircea, M., Decesari, S., Fuzzi, S., Young, J. Y., and Putaud, J. P.: Biogenically driven organic contribution to marine aerosol, *Nature*, 431, <https://doi.org/10.1038/nature02959>, 2004.
- Oppo, C., Bellandi, S., Degli Innocenti, N., Stortini, A. M., Loglio, G., Schiavuta, E., and Cini, R.: Surfactant components of marine organic matter as agents for biogeochemical fractionation and pollutant transport via marine aerosols, *Mar. Chem.*, 63, 235–253, [https://doi.org/10.1016/S0304-4203\(98\)00065-6](https://doi.org/10.1016/S0304-4203(98)00065-6), 1999.
- Pai, S. J., Heald, C. L., Pierce, J. R., Farina, S. C., Marais, E. A., Jimenez, J. L., Campuzano-Jost, P., Nault, B. A., Middlebrook, A. M., Coe, H., Shilling, J. E., Bahreini, R., Dingle, J. H., and Vu, K.: An evaluation of global organic aerosol schemes using airborne observations, *Atmos. Chem. Phys.*, 20, <https://doi.org/10.5194/acp-20-2637-2020>, 2020.
- Park, R. J., Jacob, D. J., Chin, M., and Martin, R. V.: Sources of carbonaceous aerosols over the United States and implications for natural visibility, *J. Geophys. Res.*, 108, <https://doi.org/10.1029/2002jd003190>, 2003.
- Philip, S., Martin, R. V., and Keller, C. A.: Sensitivity of chemistry-transport model simulations to the duration of chemical and transport operators: A case study with GEOS-Chem v10-01, *Geosci. Model Dev.*, 9, <https://doi.org/10.5194/gmd-9-1683-2016>, 2016.
- Philip, S., Martin, R. V., Snider, G., Weagle, C. L., Van Donkelaar, A., Brauer, M., Henze, D. K., Klimont, Z., Venkataraman, C., Guttikunda, S. K., and Zhang, Q.: Anthropogenic fugitive, combustion and industrial dust is a significant, underrepresented fine particulate matter source in global atmospheric models, *Environ. Res. Lett.*, 12, 044018, <https://doi.org/10.1088/1748-9326/aa65a4>, 2017.
- Prather, K. A., Bertram, T. H., Grassian, V. H., Deane, G. B., Stokes, M. D., DeMott, P. J., Aluwihare, L. I., Palenik, B. P., Azam, F., Seinfeld, J. H., Moffet, R. C., Molina, M. J., Cappa, C. D., Geiger, F. M., Roberts, G. C., Russell, L. M., Ault, A. P., Baltrusaitis, J., Collins, D. B., ... Zhao, D.: Bringing the ocean into the laboratory to probe the chemical complexity of sea spray aerosol, *Proc. Natl. Acad. Sci. USA*, 110, <https://doi.org/10.1073/pnas.1300262110>, 2013.
- Quinn, P. K., and Bates, T. S. (2011): The case against climate regulation via oceanic phytoplankton sulphur emissions, *Nature*, 480, 51–56, <https://doi.org/10.1038/nature10580>, 2011.
- Quinn, P. K., Coffman, D. J., Johnson, J. E., Upchurch, L. M., and Bates, T. S.: Small fraction of marine cloud condensation nuclei made up of sea spray aerosol, *Nat. Geosci.*, 10, <https://doi.org/10.1038/ngeo3003>, 2017.
- Ravishankara, A. R., Rudich, Y., Talukdar, R., and Barone, S. B.: Oxidation of atmospheric reduced sulphur compounds: Perspective from laboratory studies, *Philos. T. Roy. Soc. Lond. B.*, 352, 171–182, <https://doi.org/10.1098/rstb.1997.0012>, 1997.
- Redemann, J., Wood, R., Zuidema, P., Doherty, S. J., Luna, B., LeBlanc, S. E., Diamond, M. S., Shinzuka, Y., Chang, I. Y., Ueyama, R., Pfister, L., Ryoo, J. M., Dobracki, A. N., da Silva, A. M., Longo, K. M., Kacenelenbogen, M. S., Flynn, C. J., Pistone, K., Knox, N. M., ... Gao, L.: An overview of the ORACLES (ObseRvations of aerosols above CLOUDs and their intERactions) project: Aerosol-cloud-radiation interactions in the southeast Atlantic basin, *Atmos. Chem. Phys.*, 21, 1507–1563, <https://doi.org/10.5194/acp-21-1507-2021>, 2021.
- Russell, L. M., Hawkins, L. N., Frossard, A. A., Quinn, P. K., and Bates, T. S.: Carbohydrate-like composition of submicron atmospheric particles and their production from ocean bubble bursting, *Proc. Natl. Acad. Sci. USA*, 107, <https://doi.org/10.1073/pnas.0908905107>, 2010.
- Russell, L. M., Moore, R. H., Burrows, S. M., and Quinn, P. K.: Ocean flux of salt, sulfate, and organic components to atmospheric aerosol, *Earth-Sci. Rev.*, 239, 10.1016/j.earscirev.2023.104364, 2023.

- Ryoo, J. M., Pfister, L., Ueyama, R., Zuidema, P., Wood, R., Chang, I., and Redemann, J.: A meteorological overview of the ORACLES (ObseRvations of Aerosols above CLouds and their intEractionS) campaign over the southeastern Atlantic during 2016-2018: Part 1 – Climatology, *Atmos. Chem. Phys.*, 21, 16689–16707, <https://doi.org/10.5194/acp-21-16689-2021>, 2021.
- Seinfeld, J.H. and Pandis, S.N.: *Atmos. Chem. Phys.: From Air Pollution to Climate Change*. John Wiley and Sons, Hoboken, 2016.
- Shannon, L. V., and Nelson, G.: The Benguela: Large Scale Features and Processes and System Variability, in: *The South Atlantic*, Springer, Berlin, Heidelberg, Germany, https://doi.org/10.1007/978-3-642-80353-6_9, 1996.
- Spracklen, D. V., Carslaw, K. S., Kulmala, M., Kerminen, V. M., Sihto, S. L., Riipinen, I., Merikanto, J., Mann, G. W., Chipperfield, M. P., Wiedensohler, A., Birmili, W., and Lihavainen, H.: Contribution of particle formation to global cloud condensation nuclei concentrations, *Geophys. Res. Lett.*, 35, <https://doi.org/10.1029/2007GL033038>, 2008.
- Stier, P., Schutgens, N. A. J., Bellouin, N., Bian, H., Boucher, O., Chin, M., Ghan, S., Huneeus, N., Kinne, S., Lin, G., Ma, X., Myhre, G., Penner, J. E., Randles, C. A., Samset, B., Schulz, M., Takemura, T., Yu, F., Yu, H., and Zhou, C.: Host model uncertainties in aerosol radiative forcing estimates: Results from the AeroCom Prescribed intercomparison study, *Atmos. Chem. Phys.*, 13, <https://doi.org/10.5194/acp-13-3245-2013>, 2013.
- Su, M., Shi, Y., Yang, Y., and Guo, W.: Impacts of different biomass burning emission inventories: Simulations of atmospheric CO₂ concentrations based on GEOS-Chem, *Sci. Total Environ.*, 876, <https://doi.org/10.1016/j.scitotenv.2023.162825>, 2023.
- Swap, R., Garstang, M., Macko, S. A., Tyson, P. D., Maenhaut, W., Artaxo, P., Källberg, P., and Talbot, R.: The long-range transport of southern African aerosols to the tropical South Atlantic, *J. Geophys. Res.*, 101, <https://doi.org/10.1029/95jd01049>, 1996.
- Swap, R. J., Annegarn, H. J., Suttles, J. T., King, M. D., Platnick, S., Privette, J. L., and Scholes, R. J.: Africa burning: A thematic analysis of the Southern African Regional Science Initiative (SAFARI 2000), *J. Geophys. Res.-Atmos.*, 108, <https://doi.org/10.1029/2003jd003747>, 2003.
- Tashmim, L., Porter, W. C., Chen, Q., Alexander, B., Fite, C. H., Holmes, C. D., Pierce, J. R., Croft, B., and Ishino, S.: Contribution of expanded marine sulfur chemistry to the seasonal variability of dimethyl sulfide oxidation products and size-resolved sulfate aerosol, *Atmos. Chem. Phys.*, 24, <https://doi.org/10.5194/acp-24-3379-2024>, 2024.
- Tortell, P.D., Guéguen, C., Long, M.C., Payne, C.D., Lee, P., and DiTullio, G.R.: Spatial variability and temporal dynamics of surface water pCO₂, ΔO₂/Ar and dimethylsulfide in the Ross Sea, Antarctica. *Deep Sea Res. Part I Oceanogr. Res. Pap.*, 58, 241-259, <https://doi.org/10.1016/j.dsr.2010.12.006>, 2011.
- Tournadre, J.: Anthropogenic pressure on the open ocean: The growth of ship traffic revealed by altimeter data analysis, *Geophys. Res. Lett.*, 41, <https://doi.org/10.1002/2014GL061786>, 2014.
- Van Der Werf, G. R., Randerson, J. T., Giglio, L., Collatz, G. J., Mu, M., Kasibhatla, P. S., Morton, D. C., Defries, R. S., Jin, Y., and Van Leeuwen, T. T.: Global fire emissions and the contribution of deforestation, savanna, forest, agricultural, and peat fires (1997-2009), *Atmos. Chem. Phys.*, 10, <https://doi.org/10.5194/acp-10-11707-2010>, 2010.
- Van Der Werf, G. R., Randerson, J. T., Giglio, L., Van Leeuwen, T. T., Chen, Y., Rogers, B. M., Mu, M., Van Marle, M. J. E., Morton, D. C., Collatz, G. J., Yokelson, R. J., and Kasibhatla, P. S.: Global fire emissions estimates during 1997-2016, *Earth Syst. Sci. Data*, 9, 697–720, <https://doi.org/10.5194/essd-9-697-2017>, 2017.
- Veres, P. R., Andrew Neuman, J., Bertram, T. H., Assaf, E., Wolfe, G. M., Williamson, C. J., Weinzierl, B., Tilmes, S., Thompson, C. R., Thames, A. B., Schroder, J. C., Saiz-Lopez, A., Rollins, A. W., Roberts, J. M., Price, D., Peischl, J., Nault, B. A., Möller, K. H., Miller, D. O., ... Ryerson, T. B.: Global airborne sampling reveals a

previously unobserved dimethyl sulfide oxidation mechanism in the marine atmosphere, *Proc. Natl. Acad. Sci. USA*, 117, <https://doi.org/10.1073/pnas.1919344117>, 2020.

Vignati, E., De Leeuw, G., and Berkowicz, R.: Modeling coastal aerosol transport and effects of surf-produced aerosols on processes in the marine atmospheric boundary layer, *J. Geophys. Res.*, 106, <https://doi.org/10.1029/2000JD000025>, 2001.

Wang, X., Heald, C. L., Ridley, D. A., Schwarz, J. P., Spackman, J. R., Perring, A. E., Coe, H., Liu, D., and Clarke, A. D.: Exploiting simultaneous observational constraints on mass and absorption to estimate the global direct radiative forcing of black carbon and brown carbon, *Atmos. Chem. Phys.*, 14, <https://doi.org/10.5194/acp-14-10989-2014>, 2014.

Wizenberg, T., Strong, K., Jones, D. B. A., Lutsch, E., Mahieu, E., Franco, B., and Clarisse, L.: Exceptional wildfire enhancements of PAN, C₂H₄, CH₃OH, and HCOOH over the Canadian high Arctic during August 2017, *J. Geophys. Res.-Atmos.*, 128, <https://doi.org/10.1029/2022JD038052>, 2023.

Wood, R.: Stratocumulus clouds, *Mon. Weather Rev.*, 140, 2373–2423, <https://doi.org/10.1175/MWR-D-11-00121.1>, 2012.

Wu, R., Wang, S., and Wang, L.: New mechanism for the atmospheric oxidation of dimethyl sulfide. The importance of intramolecular hydrogen shift in a CH₃SCH₂O radical, *J. Phys. Chem. A*, 119, 112–117, <https://doi.org/10.1021/jp511616j>, 2015.

Yu, F., Luo, G., and Ma, X.: Regional and global modeling of aerosol optical properties with a size, composition, and mixing state resolved particle microphysics model, *Atmos. Chem. Phys.*, 12, <https://doi.org/10.5194/acp-12-5719-2012>, 2012.

Zhai, S., Jacob, D. J., Brewer, J. F., Li, K., Moch, J. M., Kim, J., Lee, S., Lim, H., Lee, H. C., Kuk, S. K., Park, R. J., Jeong, J. I., Wang, X., Liu, P., Luo, G., Yu, F., Meng, J., Martin, R. V., Travis, K. R., ... Liao, H.: Relating geostationary satellite measurements of aerosol optical depth (AOD) over East Asia to fine particulate matter (PM_{2.5}): insights from the KORUS-AQ aircraft campaign and GEOS-Chem model simulations, *Atmos. Chem. Phys.*, 21, <https://doi.org/10.5194/acp-21-16775-2021>, 2021.

Zhang, D., Du, L., Wang, W., Zhu, Q., Bi, J., Scovronick, N., Naidoo, M., Garland, R.M. and Liu, Y.: A machine learning model to estimate ambient PM_{2.5} concentrations in industrialized highveld region of South Africa, *Remote Sens. Environ.*, 266, 112713, 2021.

Zuidema, P., Redemann, J., Haywood, J., Wood, R., Piketh, S., Hipondoka, M., and Formenti, P.: Smoke and clouds above the southeast Atlantic: Upcoming field campaigns probe absorbing aerosol's impact on climate, *B. Am. Meteorol. Soc.*, 97, 1131–1135, <https://doi.org/10.1175/BAMS-D-15-00082.1>, 2016.

Zuidema, P., Alvarado, M., Chiu, C., de Zoete, S., Fairall, C., Feingold, G., Freedman, A., Ghan, S., Haywood, J., Kollias, P., Lewis, E., McFarquhar, G., McComiskey, A., Mechem, D., Onasch, T., Redemann, J., Romps, D., Turner, D., Wang, H., Wood, R., Yuter, S., and Zhu, P.: Layered Atlantic Smoke Interactions with Clouds (LASIC) Field Campaign Report, United States, <https://www.osti.gov/servlets/purl/1437446>, 2018.